Phytochemistry 220 (2024) 114005

Contents lists available at ScienceDirect

Phytochemistry

journal homepage: www.elsevier.com/locate/phytochem

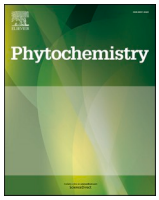

Chemical and biological investigation of *Indigofera ammoxylum* (DC.) Polhill. red and white phenotypes through feature-based molecular networking

Elise Gerometta [a,1], Elnur Garayev [b], Gaëtan Herbette [c], Arnaud Marvilliers [a], Carole Di Giorgio [d], Patricia Clerc [a], Michel Frederich [e], Béatrice Baghdikian [b], Isabelle Grondin [a], Anne Gauvin-Bialecki [a,*]

[a] Laboratoire de Chimie et de Biotechnologie des Produits Naturels, Faculté des Sciences et Technologies, Université de La Réunion, St Denis, La Réunion, France
[b] Aix Marseille Université, Avignon Université, CNRS, IRD, IMBE, Marseille, France, Faculty of Pharmacy, Service of Pharmacognosy, Marseille, France
[c] Aix-Marseille Université, CNRS, Centrale Marseille, FSCM, Spectropole, Campus de St Jérôme – Service 511, Marseille, France
[d] Aix-Marseille Université, Avignon Université, CNRS, IRD, IMBE, Marseille, France, Faculty of Pharmacy, Service of Environmental Mutagenesis, Marseille, France
[e] Université de Liège, Département de Pharmacie, Centre Interfacultaire de Recherche sur le Médicament (CIRM), Laboratoire de Pharmacognosie, Campus Du Sart-Tilman, Quartier Hôpital, Liège, Belgium

ARTICLE INFO

Keywords:
Indigofera ammoxylum
Fabaceae
Phenotype
Feature-based molecular networking
Flavonoids
Anti-inflammatory
Cytotoxic

ABSTRACT

Chemical investigation of ethyl acetate bark extracts of *Indigofera ammoxylum* red and white phenotypes led to the bio-guided isolation of four previously undescribed flavonoids, named (2*S*,3*R*)-3′,7-dihydroxy-4′,6-dimethoxyflavanol (**1**), (2*S*,3*R*)-6-methoxy-7-hydroxyflavanol (**2**), 2′,3′,7-trihydroxy-4′,6-dimethoxyisoflavone (**7**) and 2′,5' -dimethoxy-4′,5,7-trihydroxyisoflavanone (**8**), along with 14 known compounds (**3**–**6** and **9**–**18**). The previously undescribed structures were characterized based on NMR, HRESIMS, UV and IR data. Published spectroscopic data were used to deduce the structure of the known compounds. Eleven of the 18 isolated metabolites were evaluated for anti-inflammatory activity and cytotoxic activity against human liver carcinoma cells and human colon and colorectal adenocarcinoma cells. All tested compounds showed an anti-inflammatory activity (IC_{50} NO $<$ 25 μg/mL), and compounds **2** and **3** were more selective than the positive control dexamethasone. Afromorsin (**6**) showed promising cytotoxic properties against both cancer cell lines (IC_{50} 18.9 and 11.4 μg/mL). Feature-based molecular networking approach applied to bark and leaves extracts of the two phenotypes allowed to detect bioactive analogues, belonging to the families of flavones, isoflavones, flavanones, flavanols and flavonols, and to explore the chemodiversity of the species. The red and white phenotypes have a similar composition, whereas bark and leaves contain specific chemical entities. Finally, this approach highlighted a cluster of potentially bioactive and undescribed metabolites.

1. Introduction

The genus *Indigofera* (Fabaceae) includes approximately 750 species, distributed across all tropical regions and possessing a wide range of pharmacological activities such as antimicrobial, cytotoxic and anti-inflammatory properties (Gerometta et al., 2020). More than 200 metabolites are reported in this genus, including flavonoids, terpenoids and alkaloids (Gerometta et al., 2020). Some compounds have shown a potent therapeutic potential, like the anticancer bis-indole alkaloid indirubin (Gerometta et al., 2020). The species *Indigofera ammoxylum* (DC.) Polhill., commonly known as “Bois de sable”, is endemic to Reunion Island. The leaves and the bark of this species are traditionally used against diabetes, hypercholesterolemia and as a slimming remedy (Dorla et al., 2019; Técher, 2013). Previous studies showed that organic

* Corresponding author.
E-mail addresses: elise.gerometta@univ-reunion.fr (E. Gerometta), elnur.garayev@univ-amu.fr (E. Garayev), gaetan.herbette@univ-amu.fr (G. Herbette), arnaud.marvilliers@univ-reunion.fr (A. Marvilliers), carole.di-giorgio@univ-amu.fr (C. Di Giorgio), patricia.clerc@univ-reunion.fr (P. Clerc), m.frederich@uliege.be (M. Frederich), beatrice.baghdikian@univ-amu.fr (B. Baghdikian), isabelle.grondin@univ-reunion.fr (I. Grondin), anne.bialecki@univ-reunion.fr (A. Gauvin-Bialecki).
[1] Present address: Nantes Université, Institut des Substances et Organismes de la Mer, ISOMer, UR 2160, F-44000 Nantes, France.

https://doi.org/10.1016/j.phytochem.2024.114005
Received 13 September 2023; Received in revised form 25 January 2024; Accepted 26 January 2024
Available online 1 February 2024

extracts of the bark possess a strong anti-inflammatory activity, as well as antioxidant and antiviral properties (Ledoux et al., 2018; Técher, 2013). Despite these promising results, the chemical composition of the bark has never been appraised. Thus, this species was investigated in order to isolate and identify its bioactive metabolites through a bioassay-guided fractionation. In addition, a feature-based molecular networking (FBMN) approach was undertaken to detect bioactive analogues and assess the chemodiversity of the species. Indeed, two different phenotypes, named red and white phenotypes, can be found for *I. ammoxylum* and differ in juvenile leaf shape and color (Fontaine and Lavergne, 2007). So, the FBMN approach was performed in order to compare the chemical composition of these two phenotypes. Herein, the isolation, structure determination and *in vitro* anti-inflammatory and cytotoxic activities of four previously undescribed metabolites (**1**, **2**, **7** and **8**) and 14 known compounds from EtOAc (ethyl acetate) extracts of *I. ammoxylum* bark (red and white phenotypes) is reported. Results obtained from the FBMN approach are also described.

2. Results and discussion

2.1. Bio-assay guided isolation and structure determination of metabolites from the red phenotype

EtOAc extract of the bark was subjected to a solid reverse-phase extraction and yielded 3 fractions. The anti-inflammatory and cytotoxic activities of each fraction was evaluated. Fraction F1 showed a potent cytotoxic activity with IC_{50} values of 12.65 and 12.97 µg/mL against human liver carcinoma (HepG2) and human colon and colorectal adenocarcinoma (HT29) cell lines, respectively. This fraction was further purified by preparative reverse-phase HPLC and yielded two previously undescribed flavanols (**1** and **2**), along with one isoflavanone (**3**), one coumarin (**4**) and two isoflavones (**5**, reported for the first time in the genus *Indigofera*, and **6**) (Fig. 1). This is the first time compounds **3** and **4** are isolated from natural source. The metabolites **3**, **5** and **6** were identified by comparison with published spectroscopic data as 3-(2′,3’-dihydroxy-4′-methoxyphenyl)-5,7-dihydroxyisoflavanone (**3**) (Almabruk et al., 2016), pratensein (**5**) (de Almeida et al., 2008) and afromorsin (**6**) (Herath et al., 1998). Spectroscopic data of the metabolite **4**, identified as 3-(2,3-dihydroxy-4-methoxyphenyl)-7-hydroxycoumarin (**4**) (Jurd and Manners, 1977), have not been published so far and are provided here. The determination of the absolute configuration of compound **3** is also described.

2.1.1. Structure elucidation of 3′,7-dihydroxy-4′,6-dimethoxyflavanol (1)

Compound **1**, $[\alpha]_D^{25}$ −52 (*c* 0.3, MeOH) was isolated as a black solid. The HRESIMS showed a $[M+H]^+$ peak at *m/z* 319.1165 (calcd 319.1176 for $C_{17}H_{19}O_6$) (Fig. S1), suggesting the occurrence of nine degrees of unsaturation. The UV spectrum exhibited absorption maxima bands at 230 and 288 nm. The IR spectrum exhibited characteristic bands of hydroxyl groups and phenols (broad band at 3401 cm^{-1}), sp^3 type CH (2924 cm^{-1}), aromatic rings (1621 cm^{-1}), alkane type CH_2 (1442 cm^{-1}) and methyl groups (1385 cm^{-1}). The ^1H and ^{13}C NMR data (Table 1 and Figs. S2 and S3) of compound **1**, along with UV and IR data, were consistent with a flavan-3-ol derivative. The ^1H and ^{13}C NMR spectra showed signals at $\delta_{H/C}$ 6.86 (H-2′, d J = 1.6 Hz)/115.0 (C-2′), $\delta_{H/C}$ 6.90

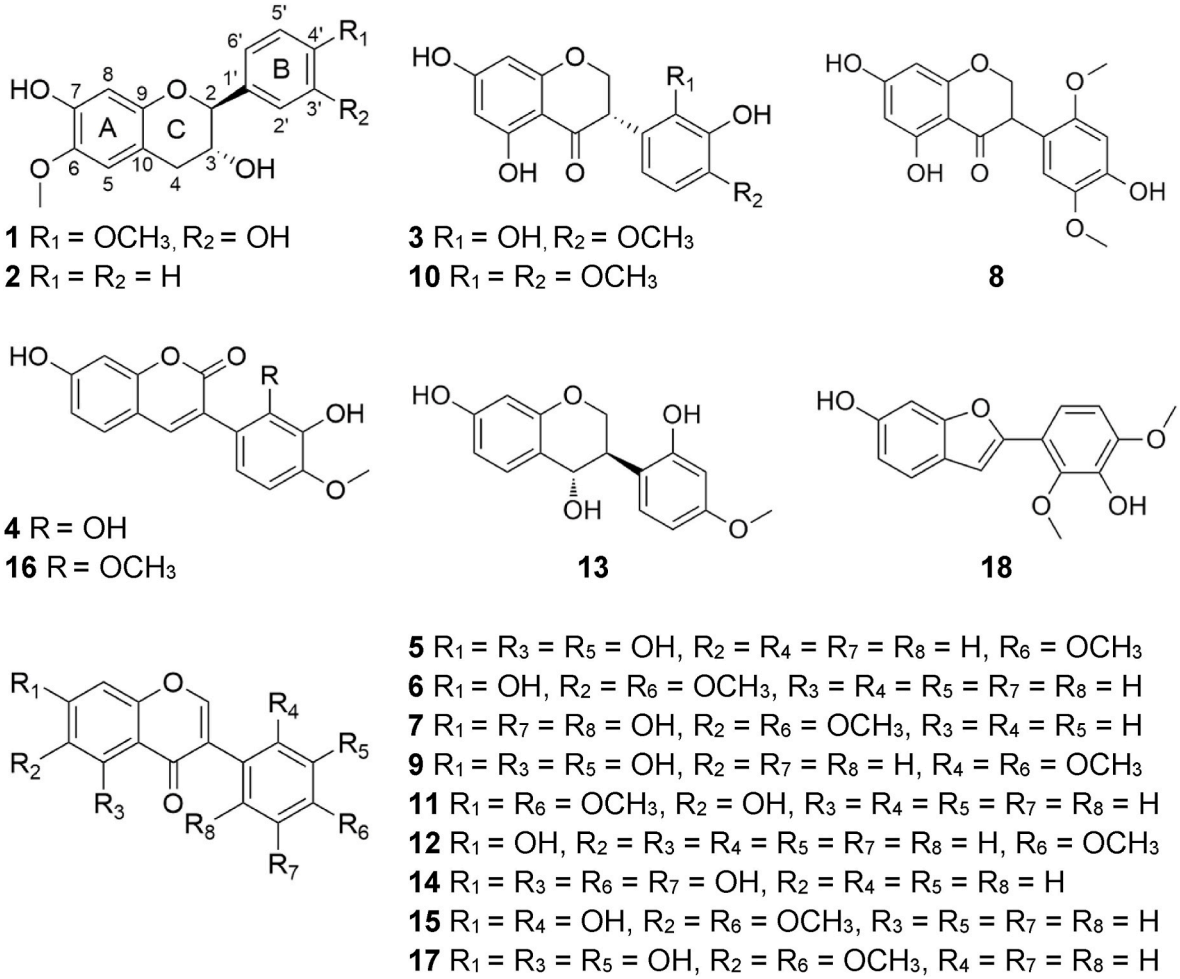

Fig. 1. Structures of compounds **1**–**18** isolated from *Indigofera ammoxylum*.

Table 1
^{1}H (600 MHz) and^{13}C (150 MHz) NMR data of compounds **1**, **2** and **4** (CD_3OD at 300 K).

No.	1		2		4	
	δ_H (mult., *J* in Hz)	δ_C, type	δ_H (mult., *J* in Hz)	δ_C, type	δ_H m (mult., *J* in Hz)	δ_C, type
2	4.62 (d, 7.2)	82.7, CH	4.73 (d, 7.4)	83.0, CH	–	163.7, CO
3	4.01 (m)	68.8, CH	4.06 (ddd, 8.4, 7.4, 5.2)	68.9, CH	–	122.9, C
4	2.88 (dd, 15.8, 5.3) 2.71 (dd, 15.8, 8.1)	33.5, CH_2	2.88 (dd, 6.0, 5.2) 2.74 (dd, 16.0, 8.4)	33.6, CH_2	7.84 (s)	144.2, CH
5	6.61 (s)	114.2, CH	6.62 (s)	114.1, CH	7.45 (d, 7.7)	130.5, CH
6	–	143.8, C	–	143.8, C	6.80 (d, 7.7)	114.6, CH
7	–	147.1, C	–	147.1, C	–	162.6, C
8	6.34 (s)	104.5, CH	6.35 (s)	104.5, CH	6.74 (brs)	103.0, CH
9	–	149.6, C	–	149.5, C	–	156.6, C
10	–	111.6, C	–	111.6, C	–	113.9, C
1′	–	133.7, C	–	140.9, C	–	117.8, C
2′	6.86 (d, 1.6)	115.0, CH	7.38 (dd, 7.3, 1.6)	128.2, CH	–	145.0, C
3′	–	147.5, C	7.35 (brt[a], 7.3)	129.3, CH	–	135.5, C
4′	–	148.9, C	7.30 (tt, 7.3, 1.6)	129.0, CH	–	149.9, C
5′	6.90 (d, 8.4)	112.5, CH	7.35 (brt, 7.3)	129.3, CH	6.55 (d, 8.3)	104.2, CH
6′	6.82 (dd, 8.4, 1.6)	119.8, CH	7.38 (dd, 7.3, 1.6)	128.2, CH	6.78 (d, 8.3)	121.7, CH
6-OCH_3	3.78 (s)	57.2, CH_3	–	57.2, CH_3	–	–
2′ - OCH_3	–	–	–	–	–	–
4′ –OCH_3	3.85 (s)	56.5, CH_3	3.79 (s)	–	3.86 (s)	56.6, CH_3
5′ –OCH_3	–	–	–	–	–	–

[a] br: broad.

(H-5′, d *J* = 8.4 Hz)/112.5 (C-5′) and $\delta_{H/C}$ 6.82 (H-6′, dd *J* = 8.4, 1.6 Hz)/119.8 (C-6′), corresponding to a 1,2,4-trisubstitued aromatic ring, and signals at $\delta_{H/C}$ 6.34 (H-8, s)/104.5 (C-8) and $\delta_{H/C}$ 6.61 (H-5, s)/114.2 (C-5), consistent with a 1,2,4,5-tetrasubstitued aromatic ring.

A shielded chemical shift was observed for carbon C-8 (δ_C 104.5), suggesting a bond to two oxygen-bearing carbons. Two signals characteristic of methoxy groups were observed at $\delta_{H/C}$ 3.78 (6-OCH_3, s)/57.2 and $\delta_{H/C}$ 3.85 (4' –OCH_3, s)/56.5. Signals observed at $\delta_{H/C}$ 2.88 (H-4a, dd *J* = 15.8, 5.3 Hz)/33.5 (C-4) and $\delta_{H/C}$ 2.71 (H-4b, dd *J* = 15.8, 8.1 Hz)/33.5 (C-4) corresponded to diastereotopic protons in *alpha* position of an aromatic ring. Finally, two deshielded signals were observed at $\delta_{H/C}$ 4.01 (H-3, m)/68.8 (C-3) and $\delta_{H/C}$ 4.62 (H-2, d *J* = 7.2 Hz)/82.7 (C-2) and corresponded to methine protons in *alpha* position of a heteroatom. The carbon signal corresponding to each proton was assigned based on HSQC experiments (Table 1 and Fig. S5). The COSY spectrum (Fig. S3) showed correlations between H-2' (δ_H 6.86), H-5' (δ_H 6.90) and H-6' (δ_H 6.82), and between H-2 (δ_H 4.62), H-3 (δ_H 4.01), H-4a (δ_H 2.88) and H-4b (δ_H 2.71), indicating two distinct spin systems corresponding to B and C ring of a flavan-3-ol, respectively. Proton H-5 (δ_H 6.61) and H-8 (δ_H 6.34) were positioned on the A ring. The linkage and the substitution pattern of these rings was determined from HMBC (Fig. 2 and Fig. S6) and NOE (Fig. 2 and Fig. S7) correlations. The HMBC correlations of H-5 (δ_H 6.61) to C-7 (δ_C 147.1), C-9 (δ_C 149.6) and C-4 (δ_C 33.5) and those of H-8 (δ_H 6.34) to C-6 (δ_C 143.8) and C-10 (δ_C 111.6) indicated the *para* position of H-5 (δ_H 6.61) and H-8 (δ_H 6.34) on an aromatic ring substituted by two oxygen in C-7 (δ_C 147.1) and C-9 (δ_C 149.6) and linked to an oxygen heterocycle, corresponding to A and C rings of the flavanol, respectively. The HMBC correlation of the methoxy protons (δ_H 3.78) to C-6 (δ_C 143.8) indicated that the aromatic ring is substituted by a methoxy group in C-6 (δ_C 143.8). This substitution was supported by the NOE correlation between methoxy protons (δ_H 3.78) and H-5 (δ_H 6.61). The HMBC correlations of H-2 (δ_H 4.62) to C-2' (δ_C 115.0) and C-6' (δ_C 119.8) and of H-2' (δ_H 6.86) to C-2 (δ_C 82.7), as well as the NOE correlations between H-2 (δ_H 4.62) and H-6' (δ_H 6.82) and between H-2 (δ_H 4.62) and H-2' (δ_H 6.86) showed that C ring is substituted by a phenyl group in C-2 (δ_C 82.7), corresponding to the B ring of the flavanol. The HMBC correlations of H-5' (δ_H 6.90) to C-3' (δ_C 147.5), of H-6' (δ_H 6.82) to C-4' (δ_C 148.9) and of methoxy protons (δ_H 3.85) to C-4' (δ_C 148.9) indicated that the B ring is substituted by a hydroxyl group in C-3' (δ_C 147.5) and a methoxy group in C-4' (δ_C 148.9). This substitution pattern was confirmed by NOE correlation between methoxy protons (δ_H 3.85) and H-5' (δ_H 6.90). Therefore, compound **1** was assigned as 3′,7-dihydroxy-4′,6-dimethoxyflavanol.

Based on NMR data, $^{3}J_{H\text{-}2/3}$ (7.2 Hz) indicated an axial-axial configuration for protons H-2 and H-3 (Liu et al., 2020), enabling the (2*R*,3*S*) or (2*S*,3*R*) configurations for (**1**). Given the double bond between C-5 and C-10, atoms 1, 4, 5 and 10 are in the same plan, implicating that the dihedral angle between protons H-2 and H-3 is not 180° but 80°. Therefore, H-2 and H-3 are in a *pseudotrans* axial-axial configuration, and a NOE correlation is observed between these two protons (Fig. S7).

2.1.2. *Structure elucidation of 6-methoxy-7-hydroxyflavanol (**2**)*

Compound **2**, $[\alpha]_D^{25}$ −51 (*c* 0.1, MeOH) was isolated as a reddish-

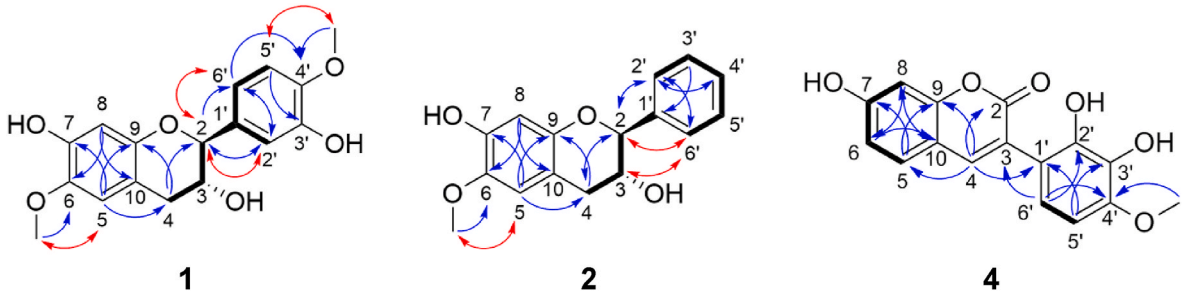

Fig. 2. Key ^{1}H–^{1}H COSY (bold), ^{1}H–^{13}C HMBC (blue arrows) and ^{1}H–^{1}H NOE (red arrows) correlations for compounds **1**, **2** and **4**. (For interpretation of the references to color in this figure legend, the reader is referred to the Web version of this article.)

brown solid. The HRESIMS showed a $[M+H]^+$ peak at *m/z* 273.1109 (calcd 273.1121 for $C_{16}H_{17}O_4$) (Fig. S8), indicating nine degrees of unsaturation. The UV spectrum exhibited absorption maxima at 295 nm. The IR spectrum exhibited characteristic bands of hydroxyl groups and phenols (broad band at 3388 cm^{-1}), sp^3 type CH (2933 cm^{-1}), aromatic rings (1605 cm^{-1}), alkane type CH_2 (1441 cm^{-1}) and methyl groups (1362 cm^{-1}). Comparison of ^1H and ^{13}C NMR data of (**2**) (Table 1 and Figs. S9 and S10) with those of (**1**) indicated similarities between these two compounds, suggesting that compound (**2**) was a 6-methoxy-7-hydroxyflavan-3-ol with an unsubstituted phenyl group as B ring. As shown in Table 1, the chemical shifts and multiplicity of H-2, H-3, H-4, H-5 and H-8 protons are almost identical for (**1**) and (**2**). Thus, the substitution pattern of rings A and C is the same for these two compounds. Signal at $\delta_{H/C}$ 7.38 (H-2′, H-6′, dd J = 7.3, 1.6 Hz)/128.2 (C-2′, C-6′), $\delta_{H/C}$ 7.35 (H-3′, H-5′, brt J = 7.3 Hz)/129.3 (C-3′, C-5′) and $\delta_{H/C}$ 7.30 (H-4′, tt J = 7.3, 1.6 Hz)/129.0 (C-4′) were consistent with an unsubstituted phenyl group, and correlations between H-2'/H-6' (δ_H 7.38), H-3'/H-5' (δ_H 7.35) and H-4' (δ_H 7.30) were observed in the COSY spectrum (Fig. S11). Therefore, compound **2** was an analogue of (**1**) and was assigned as 6-methoxy-7-hydroxyflavanol.

As for (**1**), $^3J_{H\text{-}2/3}$ (7.4 Hz) and NOE correlation indicated a *pseudo-trans* axial-axial configuration for protons H-2 and H-3 (Liu et al., 2020), enabling the (2*R*,3*S*) or (2*S*,3*R*) configurations for compound **2**.

2.1.3. Structure elucidation of 3-(2,3-dihydroxy-4-methoxyphenyl)-7-hydroxycoumarin (4)

Compound **4**, was isolated as a brown solid and showed a $[M+H]^+$ peak at *m/z* 301.0696 (calcd 301.0707 for $C_{16}H_{13}O_6$) in HRESIMS (Fig. S15), indicating 11 degrees of unsaturation. The UV spectrum exhibited absorption maxima at 250 and 341 nm. The ^1H and ^{13}C NMR (Table 1 and Figs. S16 and S17) and UV data of compound **4** were consistent with a coumarin. Indeed, the ^1H and ^{13}C NMR spectra showed a deshielded signal at $\delta_{H/C}$ 7.84 (H-4, s)/144.2 (C-4), corresponding to the proton in *beta* position of the ester function. Five aromatic signals were observed at $\delta_{H/C}$ 7.45 (H-5, d J = 7.7 Hz)/130.5 (C-5), $\delta_{H/C}$ 6.80 (H-6, d J = 7.7 Hz)/114.6 (C-6) and $\delta_{H/C}$ 6.74 (H-8, brs)/103.0 (C-8), corresponding to a 1,2,5-trisubstitued aromatic ring, and signals at $\delta_{H/C}$ 6.55 (H-5′, d J = 8.3 Hz)/104.2 (C-5′) and $\delta_{H/C}$ 6.78 (H-6′, d J = 8.3 Hz)/121.7 (C-6′), consistent with a 1,2,3,4-tetrasubstituted aromatic ring. The shielded chemical shifts observed for C-8 and C-5′ indicated a bond to one or two oxygen-bearing carbons for C-8 (δ_C 103.0) and C-5' (δ_C 104.2). Finally, one signal characteristic of a methoxy group was observed at $\delta_{H/C}$ 3.86 (4' –OCH_3, s)/56.6. The carbon signal corresponding to each proton was assigned based on HSQC experiments (Table 1 and Fig. S19). The COSY spectrum (Fig. S18) showed correlations between H-5 (δ_H 7.45), H-6 (δ_H 6.80) and H-8 (δ_H 6.74) and between H-5' (δ_H 6.55) and H-6' (δ_H 6.78), indicating two distinct spin systems corresponding to A and B ring, respectively. The linkage and the substitution pattern of these rings was determined from HMBC correlations (Fig. 2 and Fig. S20). The HMBC correlations of H-5 (δ_H 7.45) to C-7 (δ_C 162.6) and C-9 (δ_C 156.6), those of H-6 (δ_H 6.80) to C-8 (δ_C 103.0) and C-10 (δ_C 113.9) and those of H-8 (δ_H 6.74) to C-6 (δ_C 114.6) and C-10 (δ_C 113.9) indicated the *ortho* position of H-5 (δ_H 7.45) and H-6 (δ_H 6.80) and the *meta* position of H-6 (δ_H 6.80) and H-8 (δ_H 6.74) on an aromatic ring substituted by a hydroxyl group in C-7 (δ_C 162.6) and linked to an oxygen heterocycle, corresponding to A and C rings of the structure, respectively. The HMBC correlations of H-4 (δ_H 7.84) to C-9 (δ_C 156.6), C-2 (δ_C 163.7) and C-5 (δ_C 130.5) indicated the position of H-4 (δ_H 7.84) on the C ring, with an ester function in C-2 (δ_C 163.7). Based on the HMBC correlations of H-4 (δ_H 7.84) to C-1' (δ_C 117.8) and those of H-6' (δ_H 6.78) to C-3 (δ_C 122.9), the C ring was substituted by a phenyl group in C-3 (δ_C 122.9). The HMBC correlations of H-6' (δ_H 6.78) to C-3 (δ_C 122.9), C-2' (δ_C 145.0) and C-4' (δ_C 149.9), and those of H-5' (δ_H 6.55) to C-1' (δ_C 117.8) and C-3' (δ_C 135.5) indicated that H-5' (δ_H 6.55) and H-6' (δ_H 6.78) are *ortho* positioned on the phenyl group, and the latter is substituted by two hydroxy groups in C-2' (δ_C 145.0) and C-3' (δ_C 135.5). The HMBC correlations observed between the methoxy protons (δ_H 3.86) and C-4' (δ_C 149.9) indicated that the phenyl group was substituted by the methoxy group in C-4' (δ_C 149.9). Therefore, compound **4** was a coumarin and was identified as 3-(2,3-dihydroxy-4-methoxyphenyl)-7-hydroxycoumarin. This metabolite was previously described in the literature, as a synthetic derivative of sepiol (Jurd and Manners, 1977), but it is the first report of its isolation as a natural product.

2.1.4. Absolute configuration of compounds 1 and 2

For the two isomers (2*S*,3*S*) and (2*S*,3*R*), the equilibrium population of each conformer was calculated from its relative free energy using Boltzmann statistics. Thus, 14 and 16 conformers were obtained for (2*S*,3*S*) and (2*S*,3*R*), respectively (Tables S1 and S2). Experimental ^1H and ^{13}C NMR chemical shifts of compound **1** were compared with theoretical chemical shifts of the two isomers, calculated with the GIAO method at the PCM/mPW1PW91/6-31 + G (d,p) level allowing to use the DP4+ probability. The comparison was performed individually by linear regression of $\delta^1H_{theoretical} = f(\delta^1H_{experimental})$ and $\delta^{13}C_{theoretical} = f(\delta^{13}C_{experimental})$ and all together with the DP4+ probability (Table S3). When including all the data, probabilities are in favor of isomer (2*S*,3*R*) (99.68 %) (Fig. 3) which is in accordance with the *trans* axial-axial configuration established with NMR data.

To determine the absolute configuration of (**1**), ECD experimental spectrum was compared to those calculated for isomers (2*S*,3*R*) and (2*R*,3*S*). The experimental ECD spectrum of (**1**) is shown in Fig. 4. In this spectrum, wavelengths of extreme values of Cotton effect were positive around 210 and 190 nm, and negative around 200 nm. ECD spectra of the 16 populated conformers of (2*S*,3*R*) isomer were calculated at TD-wB97xd/6-311 + G (2 d,p) level. Then, a Boltzmann-weighted calculated ECD spectrum of (2*S*,3*R*) enantiomer was computed and drawn to allow comparison to the experimental spectrum. The comparison of calculated and experimental ECD spectra showed that the absolute configuration of compound **1** was found to be (2*S*,3*R*) (Fig. 4). For this enantiomer, calculated wavelengths of the positive (211 and 193 nm) and negative (201 nm) Cotton effects were in good agreement with experimental data. Therefore, compound **1** was characterized as (2*S*,3*R*)-3′,7-dihydroxy-4′,6-dimethoxyflavanol.

The absolute configuration of compound **2** was established by comparison of spectroscopic data with those reported for its analogue (**1**). Optical rotation value obtained for (**2**) ($[\alpha]_D^{25}$ −51 (*c* 0.1, MeOH)) was similar to those obtained for (**1**) ($[\alpha]_D^{25}$ −52 (*c* 0.3, MeOH)).

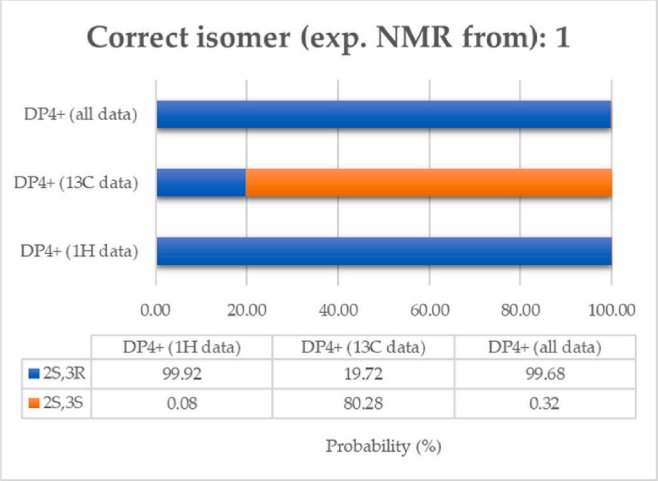

Fig. 3. Graph of ^1H-DP4+, ^{13}C-DP4+, and DP4+ (PCM/mPW1PW91/6-31 + Gdp) probabilities obtained by correlating the experimental NMR of (**1**) with the theoretical data of the two isomers (2*S*,3*R*) and (2*S*,3*S*).

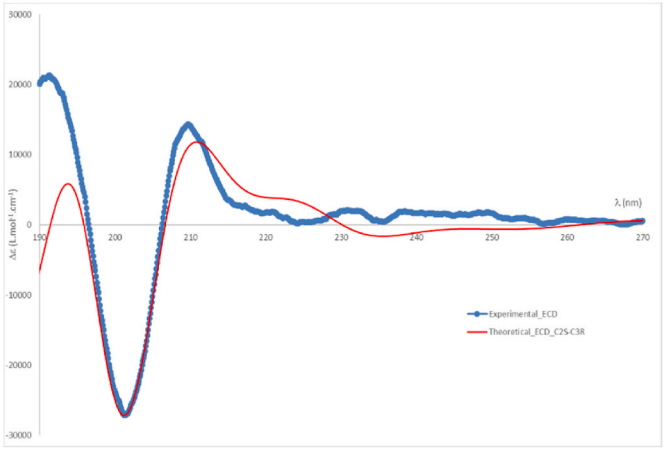

Fig. 4. ECD spectra measured (blue) in acetonitrile for (**1**) and calculated (red) using TD-wB97xd/6-311 + G (2 d,p) level for (2*S*,3*R*) isomer. (For interpretation of the references to color in this figure legend, the reader is referred to the Web version of this article.)

Consequently, this previously undescribed compound (**2**) was characterized as (2*S*,3*R*)-6-methoxy-7-hydroxyflavanol.

2.1.5. *Absolute configuration of compound **3***

Compound **3** was identified as 3-(2′,3’ -dihydroxy-4′-methoxyphenyl)-5,7-dihydroxyisoflavanone based on published spectroscopic data (Almabruk et al., 2016). So far, this isoflavanone has only been described by Almabruk et al. (2016) as a synthetic racemic mixture. Consequently, the optical rotation of (**3**) was measured and compared to the one of a close analogue, (3*R*)-dalparvine A (Umehara et al., 2008), in order to establish its absolute configuration. Optical rotation value obtained for (**3**) ($[\alpha]_D^{25}$ −12 (*c* 0.1, MeOH) was opposite to that indicated for (3*R*)-dalparvine A ($[\alpha]_D^{25}$ +15 (*c* 0.5, MeOH), indicating that compound **3** corresponds to (3*S*)-3-(2′,3’ -dihydroxy-4’ -methoxyphenyl)-5,7-dihydroxyisoflavanone.

2.2. *Bio-assay guided isolation and structure determination of metabolites from the white phenotype*

EtOAc extract of the bark was subjected to a solid reverse-phase extraction and yielded 3 fractions. The anti-inflammatory and cytotoxic activities of each fraction was evaluated. Fraction F1 showed a potent anti-inflammatory activity, with an IC_{50} value of 0.046 μg/mL and a selectivity index (SI) of 230.2 (higher than the standard drug dexamethasone), and a promising cytotoxic activity, with IC_{50} values of 15.94 and 16.03 μg/mL against HepG2 and HT29 cell lines, respectively. This fraction was further subjected to HPLC and TLC purification and yielded two undescribed isoflavonoids (**7** and **8**) (Fig. 1) and 14 compounds, including compounds **3–6**, belonging to the family of isoflavones, isoflavanones, coumarins and benzofurans. The known metabolites were identified by comparison with published spectroscopic data as khrinone C (**9**) (Umehara et al., 2009), secundiflorol H (**10**) (Tanaka et al., 1998), alfalone (**11**) (Li et al., 2008), formononetin (**12**) (Batterham and Highet, 1963), bolusanthol D (**13**) (Bojase et al., 2001), isoluteolin (**14**) (Ding et al., 2015), 6,4’ -dimethoxy-7,2′-dihydroxyisoflavone (**15**) (Belofsky et al., 2006), pterosonin F (**16**) (Su et al., 2013), iristectorigenin B (**17**) (Shawl et al., 1984) and pterofuran (**18**) (Ingham and Dewick, 1979). Compounds **9–11** and **13–18** are isolated for the first time in the genus *Indigofera*.

2.2.1. *Structure elucidation of 2′,3′,7-trihydroxy-4′,6-dimethoxyisoflavone (7)*

Compound **7**, was isolated as a beige solid and showed a $[M+H]^+$ peak at *m/z* 331.0797 (calcd 331.0812 for $C_{17}H_{15}O_7$) in HRESIMS (Fig. S21), indicating 11 degrees of unsaturation. The UV spectrum exhibited absorption maxima at 220, 261 and 324 nm. The IR spectrum exhibited characteristic bands of hydroxyl groups and phenols (broad band at 3368 cm^{-1}), sp^2 type CH (2959 cm^{-1}), sp^3 type CH (2918, 2850 cm^{-1}), aromatic rings (1594 cm^{-1}) and methyl groups (1413, 1383, 1352 cm^{-1}). The NMR (Table 2 and Figs. S22–S25), UV and IR data of (**7**) were consistent with an isoflavone. The ^{1}H NMR spectrum (Fig. S22) showed a deshielded signal at δ_H 8.12 (H-2, s), characteristic of the aromatic proton H-2 of an isoflavone pyrone ring (C ring). Two aromatic signals at δ_H 7.47 (H-5, s) and δ_H 6.74 (H-8, s) were observed. The deshielded chemical shift of H-5 (δ_H 7.47) suggested its *beta* position of the ketone function in C-4 (δ_C 178.3). Consequently, H-5 (δ_H 7.47) and H-8 (δ_H 6.74) were in a *para* configuration on the A ring of the isoflavone. Two signals were observed at δ_H 6.735 (H-6′, d J = 8.6 Hz) and δ_H 6.60 (H-5′, d J = 8.6 Hz), and the COSY spectrum (Fig. S23) showed a correlation between these two protons. H-5’ (δ_H 6.60) and H-6’ (δ_H 6.735) were then consistent with a 1,2,3,4-tetrasubstituted aromatic ring, corresponding to the B ring of the isoflavone. Two signals characteristic of methoxy groups were observed at δ_H 3.88 (4′-OCH_3, s) and δ_H 3.93 (6-OCH_3, s). The linkage and the substitution pattern of the isoflavone rings was determined from HMBC correlations (Fig. 5 and Fig. S25). The HMBC correlations of H-2 (δ_H 8.12) to C-3 (δ_C 123.6), C-4 (δ_C 178.3) and C-9 (δ_C 156.3) supported the position of this proton on the pyrone ring. The HMBC correlations of H-8 (δ_H 6.74) to C-6 (δ_C 151.4), C-9 (δ_C 156.3) and C-10 (δ_C 114.4) and of H-5 (δ_H 7.47) to C-4 (δ_C 178.3), C-6 (δ_C 151.4), C-7 (δ_C 162.6) and C-9 (δ_C 156.3) confirmed the *para* position of H-5 (δ_H 7.47) and H-8 (δ_H 6.74) on the A ring substituted by a hydroxyl group in C-7 (δ_C 162.6) and linked to the pyrone ring. The HMBC correlations of the methoxy protons (δ_H 3.93) to C-6 (δ_C 151.4) indicated the substitution of the A ring by a methoxy group in C-6 (δ_C 151.4). The HMBC correlations of H-6’ (δ_H 6.735) to C-3 (δ_C 123.6) showed that the pyrone ring was substituted by the B ring of the isoflavone in C-3 (δ_C 123.6). The HMBC correlations of H-6’ (δ_H 6.735) to C-2’ (δ_C 145.6) and C-4’ (δ_C 150.1) and of H-5’ (δ_H 6.60) to C-1’ (δ_C 115.8) and C-3’ (δ_C 136.5) indicated the substitution of the B ring by a hydroxyl group in C-2’ (δ_C 145.6) and C-3’ (δ_C 136.5). Finally, the HMBC correlations of the methoxy protons (δ_H 3.88) to C-4’ (δ_C 150.1) indicated the substitution of the B ring by a methoxy group in C-4’ (δ_C 150.1). Therefore, compound **7** was assigned as 2′,3′,7-trihydroxy-4′,6-dimethoxyisoflavone.

Table 2
^{1}H (600 MHz) and ^{13}C (150 MHz) NMR data of compounds **7** and **8** (CD_3OD at 300 K).

No.	7		8	
	δ_H (mult., *J* in Hz)	δ_C, type	δ_H (mult., *J* in Hz)	δ_C, type
2	8.12 (s)	155.4, CH	4.50 (dd, 11.6, 10.8) 4.36 (dd, 10.8, 5.6)	71.5, CH_2
3		123.6, C	4.23 (dd, 11.6, 5.6)	48.7, CH
4		178.3, C		198.8, CO
5	7.47 (s)	104.0, CH		166.0, C
6		151.4, C	5.89 (d, 2.2)	97.2, CH
7		162.6, C	–	168.7, C
8	6.74 (s)	103.7, CH	5.87 (d, 2.2)	96.1, CH
9		156.3, C	–	165.2, C
10		114.4, C	–	103.6, C
1′		115.8, C	–	114.3, C
2′		145.6, C	–	153.3, C
3′		136.5, C	6.55 (s)	101.8, CH
4′		150.1, C	–	148.6, C
5′	6.60 (d, 8.6)	105.1, CH	–	143.2, C
6′	6.735 (d, 8.6)	121.3, CH	6.74 (s)	116.2, CH
6-OCH_3	3.93 (s)	56.3, CH_3		
2′-OCH_3			3.71 (s)	56.5, CH_3
4′-OCH_3	3.88 (s)	56.6, CH_3		
5′-OCH_3			3.76 (s)	57.4, CH_3

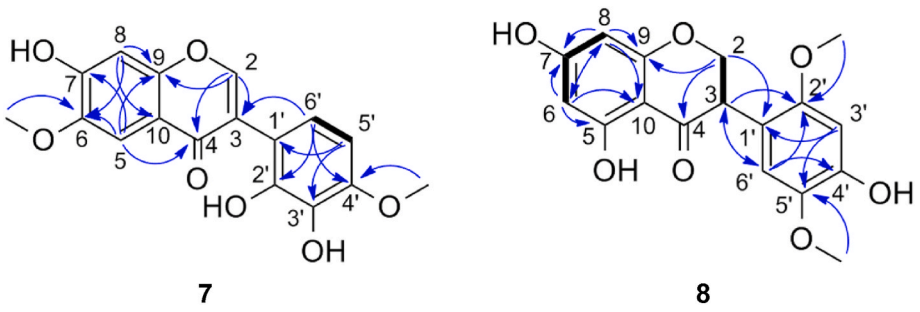

Fig. 5. Key ^{1}H–^{1}H COSY (bold) and ^{1}H–^{13}C HMBC (blue arrows) correlations for compounds **7** and **8**. (For interpretation of the references to color in this figure legend, the reader is referred to the Web version of this article.)

2.2.2. *Structure elucidation of 2′,5′-dimethoxy-4′,5,7-trihydroxyisoflavanone (**8**)*

Compound **8** was isolated as a beige solid. The HRESIMS showed a $[M+H]^+$ peak at *m/z* 333.0958 (calcd 333.0969 for $C_{17}H_{17}O_7$) (Fig. S26), indicating 10 degrees of unsaturation. The UV spectrum exhibited absorption maxima at 230 and 292 nm. The IR spectrum exhibited characteristic bands of hydroxyl groups and phenols (broad band at 3356 cm^{-1}), sp^2 type CH (2956 cm^{-1}), sp^3 type CH (2921, 2851 cm^{-1}), a ketone function (1724 cm^{-1}), aromatic rings (1633, 1601 cm^{-1}), alkane type CH_2 (1511, 1485, 1465 cm^{-1}) and methyl groups (1427, 1378 cm^{-1}). The NMR (Table 2 and Figs. S27–S30), UV and IR data of (**8**) were consistent with an isoflavanone. The ^{1}H NMR spectrum (Fig. S27) showed two signals at δ_H 5.89 (H-6, d $J = 2.2$ Hz) and δ_H 5.87 (H-8, d $J = 2.2$ Hz), corresponding to a 1,2,3,5-tetrasubstituted aromatic ring. The shielded chemical shifts observed for C-6 (δ_C 97.2) and C-8 (δ_C 96.1) suggested an *alpha* position of two oxygen-bearing carbons for these two carbons. Signals observed at $\delta_{H/C}$ 6.74 (H-6′, s)/116.2 (C-6′) and at $\delta_{H/C}$ 6.55 (H-3′, s)/101.8 (C-3′) were consistent with a 1,2,4,5-tetrasubstituted aromatic ring. The shielded chemical shift observed for C-3′ (δ_C 101.8) indicated its *alpha* position of two oxygen-bearing carbons. Two signals characteristic of methoxy groups were observed at $\delta_{H/C}$ 3.76 (5′-OCH_3, s)/57.4 and $\delta_{H/C}$ 3.71 (2′-OCH_3, s)/56.5. Signals observed at $\delta_{H/C}$ 4.50 (H-2a, dd $J = 11.6$, 10.8 Hz)/71.5 (C-2) and $\delta_{H/C}$ 4.36 (H-4b, dd $J = 10.8$, 5.6 Hz)/71.5 (C-2) corresponded to diastereotopic protons in *alpha* position of a heteroatom. A deshielded signal was observed at $\delta_{H/C}$ 4.23 (H-3, dd $J = 11.6$, 5.6 Hz)/48.7 (C-3) and corresponded to a proton in *alpha* position of an aromatic ring. The COSY spectrum (Fig. S28) showed correlations between H-6 (δ_H 5.89) and H-8 (δ_H 5.87), and between H-2a (δ_H 4.50), H-2b (δ_H 4.36) and H-3 (δ_H 4.23), indicating two distinct spin systems corresponding to A and C ring of the isoflavanone, respectively. Proton H-3' (δ_H 6.55) and H-6' (δ_H 6.74) were positioned on the B ring. The linkage and the substitution pattern of these rings was determined from HMBC correlations (Fig. 5 and Fig. S30). The HMBC correlations of H-6 (δ_H 5.89) to C-5 (δ_C 166.0), C-7 (δ_C 168.7), C-8 (δ_C 96.1) and C-10 (δ_C 103.6) and of H-8 (δ_H 5.87) to C-6 (δ_C 97.2), C-7 (δ_C 168.7), C-9 (δ_C 165.2) and C-10 (δ_C 103.6) supported the *meta* configuration of these two protons on the A ring, substituted by two hydroxyl groups in C-5 and C-7. The HMBC correlations of H-2a/H-2b (δ_H 4.50/4.36) to C-4 (δ_C 198.8) and C-9 (δ_C 165.2) confirmed the position of these two protons in C-2 (δ_C 71.5) on the C ring. The HMBC correlations of H-2a/H-2b (δ_H 4.50/4.36) to C-1' (δ_C 114.3), of H-3 (δ_H 4.23) to C-2' (δ_C 153.3) and C-6' (δ_C 116.2), and of H-6' (δ_H 6.74) to C-3 (δ_C 48.7) supported the position of the B ring in C-3. The HMBC correlations of H-3' (δ_H 6.55) to C-1' (δ_C 114.3) and C-5' (δ_C 143.2), and of H-6' (δ_H 6.74) to C-1' (δ_C 114.3), C-2' (δ_C 153.3) and C-4' (δ_C 148.6) indicated the *para* configuration of these two protons on the B ring, substituted by a hydroxy group in C-4' (δ_C 148.6). The HMBC correlation of the methoxy protons at δ_H 3.76 to C-5' (δ_C 143.2) and of the methoxy protons at δ_H 3.71 to C-2' (δ_C 153.3) indicated that the B ring is substituted by two methoxy groups in C-5' (δ_C 143.2) and C-2' (δ_C 153.3). Therefore, (**8**) was characterized as 2′,5′-dimethoxy-4′,5,7-trihydroxyisoflavanone. It was isolated as a mixture with several unidentified minor compounds. Thus, its absolute configuration has not been established.

2.3. *Evaluation of the in vitro anti-inflammatory and cytotoxic activity of the isolated compounds*

Isolated compounds were tested for *in vitro* anti-inflammatory and cytotoxic activities. Due to their paucity, the previously undescribed compounds **7** and **8** and known compounds **14**, **15**, **16** and **18** were not evaluated. The purity of the tested compounds was evaluated based on CAD chromatograms and NMR data. Compounds **2**, **4** and **10** are more than 90 % pure, compounds **1**, **3**, **6**, **11** and **13** are more than 80 % pure, and compounds **5**, **9** and **12** are between 60 and 70 % pure. Anti-inflammatory activity was assessed through a mouse macrophage RAW 264.7 model. The capacity of compounds to inhibit nitric oxide (NO) production was measured (IC_{50} NO). Their cytotoxicity (IC_{50}) towards mouse macrophages was evaluated in order to determine their selectivity index (SI) (IC_{50}/IC_{50} NO ratio).

Ten of the eleven tested compounds displayed a significant anti-inflammatory activity ($IC_{50} < 15$ μg/mL). Compounds **2**, **3** and **9** showed a high selectivity, higher than the standard drug for **2** and **3** (Table 3). The cytotoxic properties of the compounds were evaluated on HepG2 and HT29 cancer cell lines, through the Red Dye assay. The four compounds **1**, **4**, **11** and **12** showed a moderate cytotoxicity against one or both cell lines ($IC_{50} < 50$ μg/mL) (Table 3). Compound **6** displayed a relevant activity against both cell lines, with an IC_{50} value of 18.92 and 11.36 μg/mL against HepG2 and HT29 cell lines, respectively.

2.4. *Feature-based molecular networking*

A feature-based molecular networking (Nothias et al., 2020) approach was performed in order to (1) provide additional information about the phytochemistry of *I. ammoxylum*, (2) compare the chemical composition of the different phenotypes and different plant parts of the species and (3) detect clusters, with features present in extracts with selective anti-inflammatory activity. For this purpose, leaves and bark EtOAc crude extracts of the two phenotypes of *I. ammoxylum* were subjected to an UHPLC-HRESIMS/MS analysis and a molecular network (MN) was generated with the FBMN tool on the GNPS platform.

A MN comprising 1196 nodes and 50 clusters (three nodes at least) was obtained (Fig. 6). In Fig. 6a, squared pink nodes correspond to the isolated compounds **1**–**3**, **5**–**7**, **10**–**11** and **18**, and green nodes correspond to spectral matches on GNPS or ISDB databases. The edges thickness correlates with the cosine score (CS) value (0.7–1) between two nodes. Based on spectral matches, the largest cluster C1 corresponds to fatty acids and fatty acids derivatives. Nodes included in cluster C2 correspond to glycosylated flavonols and isoflavonols, and more particularly to glycosylated derivatives of quercetin, four of which correspond to metabolites reported previously in *Indigofera* species: kaempferin (Luiz-Ferreira et al., 2012), quercitrin (Rahman et al., 2015),

Table 3
Anti-inflammatory and cytotoxic activity of the fractions and isolated compounds.

Fraction	Compound	Anti-inflammatory activity[a]		Cytotoxic activity[b]	
		IC_{50} NO (μg/mL)	SI	IC_{50} HepG2 (μg/mL)	IC_{50} HT29 (μg/mL)
Red phenotype – F1	–	0.65 ± 0.09	12.90	12.65 ± 3.84	12.94 ± 3.08
	1	4.65 ± 2.21	9.30	36.27 ± 2.08	44.94 ± 2.65
	2	23.36 ± 1.55	428.00	>100	>100
	3	0.11 ± 0.05	793.27	>50	>50
	4	5.09 ± 1.06	9.86	46.09 ± 3.17	>50
	5	3.27 ± 0.92	14.52	>50	>50
	6	1.03 ± 0.12	13.27	18.92 ± 1.04	11.36 ± 2.08
White phenotype – F1	–	0.046 ± 0.008	230.20	15.94 ± 3.84	16.03 ± 3.28
	9	1.78 ± 0.23	38.69	>50	>50
	10	3.89 ± 0.64	12.06	51.56 ± 3.26	56.36 ± 2.67
	11	9.81 ± 1.12	2.94	42.92 ± 1.93	38.03 ± 2.38
	12	3.21 ± 0.76	6.71	33.34 ± 2.12	45.34 ± 3.43
	13	8.26 ± 1.86	8.03	56.34 ± 4.25	61.33 ± 4.09
Dexamethasone	–	4.05 ± 0.78	45.51	–	–

[a,b] IC_{50} are the means ± standard deviations calculated from three independent assays.

nicotiflorin (Elmi et al., 2018) and quercetin-3-*O*-[-β-D-glucopyranosyl-(1 → 2)-β-D-glucopyranoside] (Campos et al., 2018). Cluster C3 is a cluster of terpenes and terpenoids, including betulinic acid, a triterpene reported in the species *Indigofera carlesii* (Zhang et al., 2006).

Cluster C5 contains the isolated compounds **3** (*m/z* 319.0807), **7** (*m/z* 331.0806) and **10** (*m/z* 333.096), and corresponds to flavonoids and isoflavonoids, more precisely to flavones/isoflavones and flavanones/isoflavanones. In the present work, compound **3** showed a potent and selective anti-inflammatory activity (Table 3). Based on structure-activity relationship, the nodes connected to compound **3** could fit with selective anti-inflammatory analogues. Two nodes correspond to particularly close analogues of (**3**): nodes at *m/z* 333.096 (CS = 0.90) and *m/z* 317.065 (CS = 0.93). Based on ISDB, these nodes matched 3,5,7-trihydroxy-4′,8-dimethoxyflavanone and 3,5,6,7-tetrahydroxy-4′-methoxyflavone, respectively.

Cluster C12 is a cluster of flavanols and flavonols, and contain the isolated compounds **1** (*m/z* 319.1169) and **2** (*m/z* 273.1118). Based on GNPS matches, two other nodes have been identified as epigallocatechin and epicatechin. The latter has been previously reported in the species *Indigofera aspalathoides* (Sundarrajan and Arumugam, 2017). Two nodes, at *m/z* 319.1163 (CS = 0.85) and *m/z* 305.1009 (CS = 0.88), correspond to close analogues of compound **2**, for which a potent selective anti-inflammatory activity has been shown in the present work. The annotation of these two nodes based on ISDB matches is not consistent with the observed CS values. These two analogues remain unidentified.

Cluster C23 includes the isolated compound **18** (*m/z* 287.0906). Due to its paucity, biological activity of this metabolite has not been appraised in this work, but its cytotoxic properties have been previously reported (Su et al., 2017). Consequently, cluster C23 could contain cytotoxic analogues. A high CS value (CS = 0.90) is observed between the node of (**18**) and a node at *m/z* 271.0956, identified as stemofuran D based on ISDB matches. This compound had never been reported in the Fabaceae family so far, and possesses anti-inflammatory properties (Shen et al., 2013).

Cluster C24 is a cluster of flavones and isoflavones. The node at *m/z* 301.0703 corresponds to the isolated compound **5**, which showed good anti-inflammatory properties in the present work (Table 3). Two nodes at *m/z* 285.0754 and *m/z* 285.0752 are two close analogues of **5** (CS = 0.91). Based on GNPS matches, one of them could correspond to calycosin, an isoflavone reported in numerous Fabaceae species with proved anti-inflammatory activity (Su et al., 2016).

Cluster C31 comprises four nodes corresponding to flavones and isoflavones. The two isomeric isolated isoflavones **6** and **11** are found in this cluster. In the present work, compound **6** showed interesting anti-inflammatory and cytotoxic properties (Table 3), thus cluster C31 could contain anti-inflammatory and cytotoxic analogues. Based on GNPS matches, a node at *m/z* 285.0753 was annotated as biochanin A, an isoflavone particularly common in the Fabaceae genera *Trifolium* and *Cicer*. Cytotoxic (Cho et al., 2017) and anti-inflammatory (Felix et al., 2021) activities are reported for this metabolite.

The FBMN approach provided some information about the chemodiversity of the species *I. ammoxylum*. Almost all nodes from the red phenotype were shared with those from the white phenotype, indicating a similar qualitative composition for both phenotypes. The compounds isolated in this work are present in both phenotypes, except (**16**) which is only found in the white phenotype. In Fig. 6b, the pie chart represents the peak area corresponding to each node in the LC/MSMS spectra. Green-filled nodes correspond to nodes from the leaves extracts and brown-filled nodes to nodes from the bark extract. Some clusters or part of clusters contain nodes that exclusively relate to the bark extracts, whereas others contain nodes that relate exclusively to the leaves extracts, indicating a distinctive composition between these two parts of plant. Based on annotations, the bark extracts specifically contain triterpenoids, isoflavones, isoflavanones and flavanols, whereas leaves extracts contain quercetin glycosylated derivatives and alkaloids. Most of the isolated compounds are only present in the bark extracts, but compounds **2**, **11**, **13** and **15** are also found in the leaves extracts.

The anti-inflammatory activity of the four crude extracts was evaluated, and two extracts showed a very potent activity and selectivity: the bark extract of the white phenotype (IC_{50} NO = 0.046 μg/mL, SI = 3106.6) and the leaves extract of the red phenotype (IC_{50} NO = 0.043 μg/mL, SI = 3206.9). The two other extracts showed a good activity (IC_{50} NO < 2 μg/mL) but a poor selectivity (SI < 40). The FBMN approach was performed in order to highlight exclusive clusters of the selective extracts and therefore to explain this difference of activity and to detect the active and selective metabolites (Olivon et al., 2017a). In Fig. 6b, the border of the nodes displays the biological activity of the extracts. Red-bordered nodes are from anti-inflammatory and selective extracts, and blue-bordered nodes are from anti-inflammatory but non-selective extracts. No exclusive cluster of the two selective extracts was observed. Nevertheless, some clusters like the cluster C15 (Figs. 6b and 7) contain nodes mainly related to selective extracts, and particularly to the white phenotype bark extract. Based on ISDB matches, this cluster could correspond to glycosylated phenolic compounds. Anti-inflammatory properties of such compounds are reported in the literature (Küpeli et al., 2007), so this cluster could partially explain the important and selective activity of the white phenotype bark extract. It would be interesting to target the isolation of these metabolites, to identify them and evaluate their pharmacological properties.

3. Conclusions

In conclusion, 18 metabolites were isolated from the EtOAc bark extracts of *I. ammoxylum* red and white phenotypes. Compounds **1–4**, **7** and **8** are previously undescribed natural products. This is the first report of compounds **5**, **9–11** and **13–18** in the genus *Indigofera*. All the

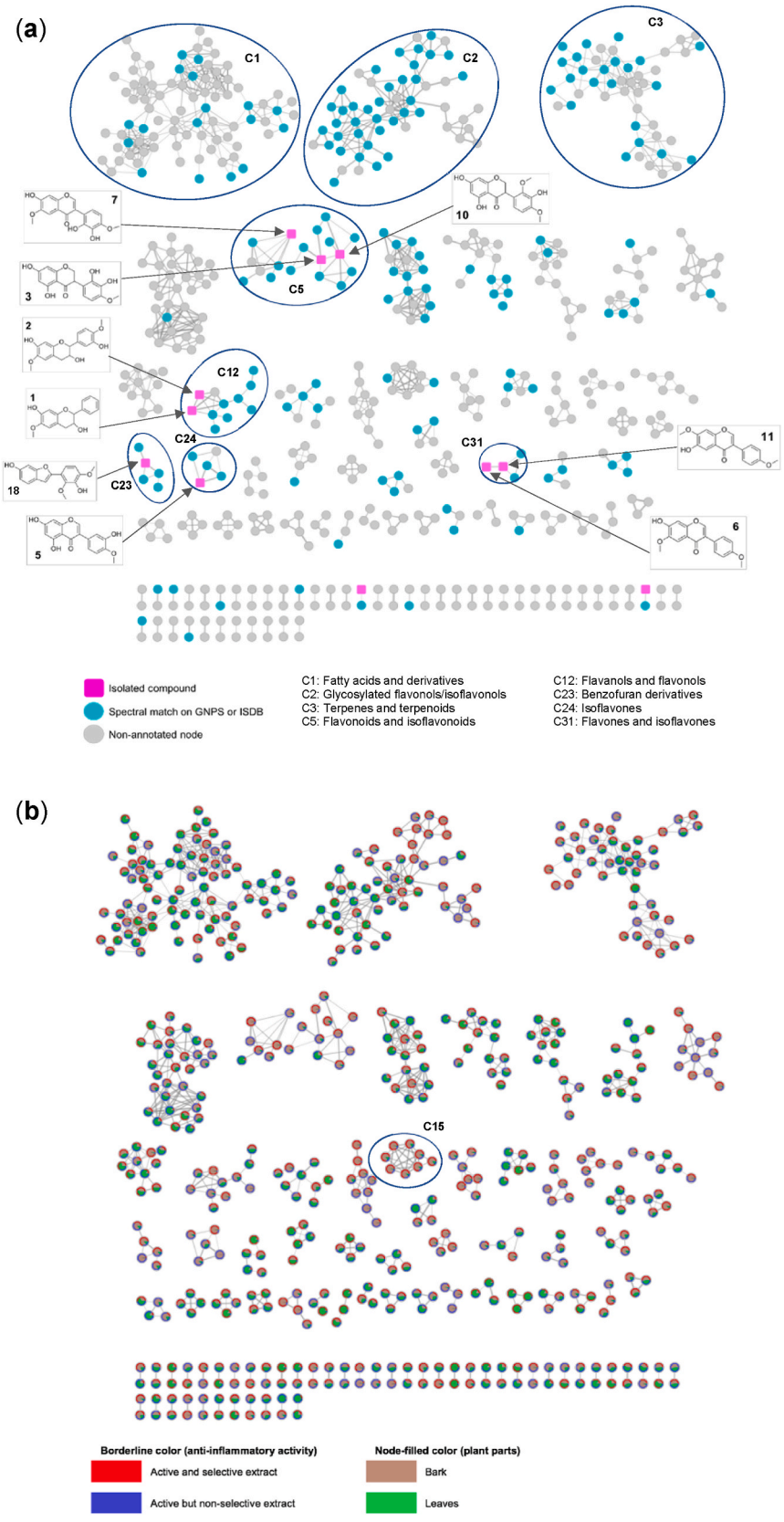

Fig. 6. (**A**) Molecular network (MN) of the isolated compounds (pink squared nodes) and MN annotation based on GNPS and ISDB spectral matches (round green nodes). (**b**) Repartition of the two plant parts (bark and leaves) extracts and selective and non-selective anti-inflammatory extracts in the MN. (For interpretation of the references to color in this figure legend, the reader is referred to the Web version of this article.)

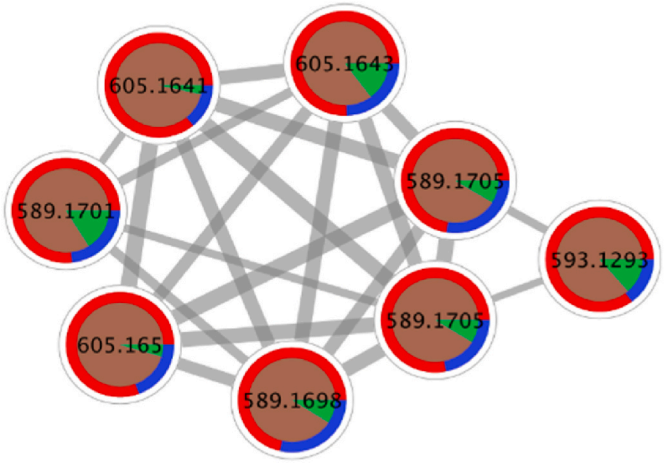

Fig. 7. Cluster C15 of the MN, containing nodes mostly related to anti-inflammatory and selective extracts (red bordered nodes). (For interpretation of the references to color in this figure legend, the reader is referred to the Web version of this article.)

tested compounds except (**2**) showed a high anti-inflammatory activity (IC_{50} < 10 μg/mL). Compounds (**2**), (**3**) and (**9**) demonstrated an interesting selectivity (SI > 30), and the SI of (**2**) and (**4**) was higher than the one of the positive control. Compound **6** showed promising cytotoxic properties against HepG2 and HT29 cancer cell lines. The FBMN approach allowed the detection of bioactive analogues, and some of them have been putatively identified as stemofuran D, biochanin A and calycosin. Regarding the chemodiversity of the species, the red and white phenotypes have a similar composition but bark and leaves contain specific chemical entities. Finally, no exclusive cluster of the most active and selective extracts was detected, but a cluster of apparently undescribed glycosylated phenolic compounds could explain the selectivity of the white phenotype bark extract and should be isolated and identified in a future work.

4. Experimental

General Experimental Procedures. Optical rotations were determined using an Anton Paar MCP200 polarimeter (589 nm, 25 °C), and UV spectra were acquired on a Thermo Scientific DAD spectrophotometer. IR spectra were recorded on a Vertex 70 (Bruker) ATR-FTIR spectrometer. For compound **1**, experimental ECD spectrum was recorded on a JASCO J-815 spectrometer equipped with a JASCO Peltier cell holder PTC-423 to maintain the temperature at 20.0 °C. The handedness of the circular polarized light was modulated at 50 kHz with a quartz photoelastic modulator set at ¼ retardation. A quartz cell of 1 mm of optical path length was used. Sample was prepared in acetonitrile at a concentration of 0.0003 mol.L^{-1}. NMR spectra were acquired in CD_3OD on either a Bruker Avance III 600 MHz (TXI probe) or a Bruker Avance II^+ 600 MHz (TCI cryoprobe) spectrometer and were analyzed with the TopSpin (v 4.1.1) software. The chemical shifts δ are given in ppm and coupling constants J in Hz. UHPLC-HRESIMS and UHPLC-HRESIMS/MS analysis were performed on an Impact II Bruker Daltonics Qq-TOF spectrometer with an ESI source, using a 2.1 × 150 mm 1.6 μm RP-C_{18} column (Luna Omega C18, Phenomenex) and an elution gradient of H_2O–CH_3CN with 0.1 % HCO_2H (98:2 to 0:100). Solid reverse-phase extraction was performed over 10 g SPE Strata 55 μm C18 tubes (Phenomenex), with three elution steps (H_2O/CH_3CN *v/v*). Preparative HPLC were performed on a Waters 2545 system using MassLynx software and a 21.2 × 150 mm 5 μm RP-C_{18} column (Gemini C18, Phenomenex), with an appropriate elution gradient of H_2O–CH_3CN with 0.1 % HCO_2H at a flow rate of 20 mL/min and on a PLC 2020 Gilson system using a 4.6 × 250 mm 5 μm PFP column (Luna PFP Phenomenex) and an elution system of H_2O–CH_3CN with 0.1 % HCO_2H (70:30) for 40 min at a flow rate of 0.8 mL/min. Preparative TLC were performed on glass plates (20 × 20 cm) precoated with silica gel 60 F_{254} (2 mm) (Merck). After two successive developments with appropriate solvent systems, revealing of the plates was performed under UV light (254 and 366 nm). All solvents were analytical or HPLC grade.

Plant material. Leaves and bark of the red and white phenotypes of *Indigofera ammoxylum* were collected in March and April 2019 in Reunion Island (Saint Denis). The taxonomic identification of the plant species was performed by Mr. H. Thomas (Parc National de La Réunion). For each phenotype, a voucher specimen was deposited in the Herbarium of the University of La Réunion for confirmation of identification, and the accession numbers REU024077 (red phenotype) and REU024078 (white phenotype) were attributed to the samples.

Extraction and isolation. Leaves and bark of *I. ammoxylum* were dried at 40 °C for 48 h and powdered. Samples of 228.0 g (leaves) and 74.0 g (bark) were obtained from the red phenotype, and samples of 240.0 g (leaves) and 247.3 g (bark) from the white phenotype. The ground materials were extracted exhaustively using an accelerated solvent extractor (ASE 300 Dionex). Four successive extractions were performed at 40 °C with EtOAc for each sample. The extracts were evaporated under reduced pressure at 38 °C to obtain 8.4 g (leaves) and 3.1 g (bark) of crude extracts for the red phenotype and 8.2 g (leaves) and 7.7 g (bark) of crude extracts for the white phenotype. 1.26 g of the red phenotype bark crude extract were fractionated by solid reverse-phase extraction using combinations of H_2O/CH_3CN (*v/v*) of decreasing polarity. Three fractions (F1–F3) were obtained and evaluated for their anti-inflammatory and cytotoxic activity. All fractions showed a potent anti-inflammatory activity (IC_{50} = 0.68, 0.48 and 0.13 μg/mL, respectively) and fraction F2 showed a high selectivity (SI = 100.1) compared to the standard drug dexamethasone. Fraction F1 showed a promising cytotoxic activity against HepG2 and HT29 cell lines, with IC_{50} values of 12.65 and 12.97 μg/mL, respectively. Fraction F1 (513.8 mg) was then subjected to preparative HPLC, using an elution gradient of H_2O–CH_3CN with 0.1 % HCO_2H (80:20 over 2 min, 80:20 to 52:48 over 30 min) at a flow rate of 20 mL/min (UV 230 nm). The purification of fraction F1 afforded the compounds (2*S*,3*R*)-3′,7-dihydroxy-4′,6-dimethoxyflavanol (**1**, 4.9 mg), (2*S*,3*R*)-6-methoxy-7-hydroxyflavanol (**2**, 6.9 mg), 3-(2′,3′-dihydroxy-4′-methoxyphenyl)-5,7-dihydroxyisoflavanone (**3**, 8.8 mg), 3-(2,3-dihydroxy-4-methoxyphenyl)-7-hydroxycoumarin (**4**, 15.1 mg), pratensein (**5**, 12.4 mg) and afromorsin (**6**, 8.4 mg). 2.7 g of the white phenotype bark crude extract were fractionated by solid reverse-phase extraction using combinations of H_2O/CH_3CN (*v/v*) of decreasing polarity. Three fractions (F1–F3) were obtained and evaluated for their anti-inflammatory and cytotoxic activity. A potent anti-inflammatory activity was observed for the three fractions (IC_{50} values of 0.046, 0.22 and 0.35 μg/mL, respectively), but only fraction F1 displayed a high selectivity (SI = 230.2) compared to the standard drug. Fraction F1 showed a promising cytotoxic activity against HepG2 and HT29 cell lines, with IC_{50} values of 15.94 and 16.03 μg/mL, respectively. Fraction F1 (582.9 mg) was then subjected to preparative HPLC, using an elution gradient of H_2O–CH_3CN with 0.1 % HCO_2H (80:20 over 2 min, 80:20 to 47:53 over 24 min) at a flow rate of 20 mL/min (UV 230 nm). The purification of fraction F1 led to the isolation of the compounds 3-(2′,3′-dihydroxy-4′-methoxyphenyl)-5,7-dihydroxyisoflavanone (**3**, 6.4 mg), afromorsin (**6**, 11.4 mg), khrinone C (**9**, 16.3 mg), secundiflorol H (**10**, 19.7 mg) and bolusanthol D (**13**, 8.9 mg). Subfraction F1-2 (13.3 mg) was subjected to preparative TLC purification. After two successive developments with a solvent system of $CHCl_3$/MeOH 97/3 (*v/v*), the plate was revealed under UV light (254 and 366 nm). The compounds 3-(2,3-dihydroxy-4-methoxyphenyl)-7-hydroxycoumarin (**4**, 0.54 mg), 2′,3′,7-trihydroxy-4′,6-dimethoxyisoflavone (**7**, 0.2 mg) and isoluteoline (**14**, 0.04 mg) were thus obtained and recovered with EtOAc. The purification of subfraction F1-4 (7.2 mg) was performed by analytical HPLC using an isocratic elution of H_2O–CH_3CN with 0.1 % HCO_2H (70:30) for 40 min at a flow rate of 0.8 mL/min (UV 280 nm), and yielded the

compounds 3-(2′,3′-dihydroxy-4′-methoxyphenyl)-5,7-dihydroxyisoflavanone (**3**, 0.2 mg) and pterosonin F (**16**, 0.08 mg). Subfractions F1-7 (11.7 mg) and F1-9 (18.4 mg) were subjected to preparative TLC purification. After two successive developments with a solvent system of Toluene/MeOH 90/10 (*v/v*), the plates were revealed under UV light (254 and 366 nm) and the compounds recovered with EtOAc. Subfraction F1-7 afforded the four compounds pratensein (**5**, 0.18 mg), 2′,5′-dimethoxy-4′,5,7-trihydroxyisoflavanone (**8**, 0.26 mg), 6,4′-dimethoxy-7,2′-dihydroxyisoflavone (**15**, 0.32 mg) and iristectorigenin B (**17**, 0.10 mg), and subfraction F1-9 yielded compounds alfalone (**11**, 0.42 mg), formononetin (**12**, 0.44 mg) and pterofuran (**18**, 0.38 mg).

(2*S*,3*R*)-3′,7-dihydroxy-4′,6-dimethoxyflavanol (**1**): black solid; $[\alpha]_D^{25}$ −52 (*c* 0.3, MeOH); UV (MeOH) λ_{max} 230, 288 nm; IR ν_{max} 3401, 2924, 1621, 1515, 1442, 1385, 1273, 1164, 1123, 1029 cm^{-1}; for ^1H and ^{13}C NMR data, see Table 1; HRESIMS *m/z* 319.1165 $[M+H]^+$ (calcd for $C_{17}H_{19}O_6$, 319.1176).

(2*S*,3*R*)-6-methoxy-7-hydroxyflavanol (**2**): reddish-brown solid; $[\alpha]_D^{25}$ −51 (*c* 0.3, MeOH); UV (MeOH) λ_{max} 295 nm; IR ν_{max} 3388, 2933, 2845, 1605, 1512, 1441, 1362, 1282, 1235, 1157, 1124, 1028 cm^{-1}; for ^1H and ^{13}C NMR data, see Table 1; HRESIMS *m/z* 273.1109 $[M+H]^+$ (calcd for $C_{16}H_{17}O_4$, 273.1121).

3-(2,3-dihydroxy-4-methoxyphenyl)-7-hydroxycoumarin (**4**): brown solid; UV λ_{max} 250, 341 nm; for ^1H and ^{13}C NMR data, see Table 1; HRESIMS *m/z* 301.0696 $[M+H]^+$ (calcd for $C_{16}H_{13}O_6$, 301.0707).

2′,3′,7-trihydroxy-4′,6-dimethoxyisoflavone (**7**). Beige solid; UV λ_{max} 220, 261, 324 nm; IR ν_{max} 3368, 2959, 2918, 2850, 1594, 1413, 1383, 1352, 1260, 1180, 1101, 1046 cm^{-1}; for ^1H and ^{13}C NMR data, see Table 2; HRESIMS *m/z* 331.0797 $[M+H]^+$ (calcd for $C_{17}H_{15}O_7$, 331.0812).

2′,5′-dimethoxy-4′,5,7-trihydroxyisoflavanone (**8**). Beige solid; UV λ_{max} 230, 292 nm; IR ν_{max} 3356, 2956, 2921, 2851, 1724, 1633, 1601, 1511, 1485, 1465, 1427, 1378, 1266, 1193, 1164, 1098, 1037 cm^{-1}; for ^1H and ^{13}C NMR data, see Table 2; HRESIMS *m/z* 333.0958 $[M+H]^+$ (calcd for $C_{17}H_{17}O_7$, 333.0969).

Molecular modelling. All DFT calculations were carried out using the GAUSSIAN 09 program (Frisch et al., 2013) using the hybrid B3LYP exchange-correlation functional (Becke, 1993; Stephens et al., 1994) and the 6-31 + G (d,p) basis set. Tight convergence criteria were used for geometry optimization. All stationary points were confirmed as true minima *via* vibrational frequency calculations. Frequencies calculated in the harmonic approximation were multiplied with a factor set to 0.98. NMR shielding tensors were computed with the Gauge-Independent Atomic Orbital (GIAO) method (Cheeseman et al., 1996). The calculated nuclear isotropic magnetic shieldings (IMS) were converted for carbons C–i into chemical shifts by referencing to tetramethylsilane (TMS) IMS calculated at the same level of theory (IMSTMS = 197.2863 ppm); and for hydrogens H-i into chemical shifts (IMSTMS = 31.6175 ppm): d_corr = IMSTMS - IMSC–i. Electronic excitation energies and rotational strengths for all conformations have been calculated using the TD-DFT methodology of Gaussian 09 for the 100 lowest singlet vertical excitation energies at ground-state equilibrium geometries. Thence ECD spectra were obtained assuming the Condon approximation and the computed velocity rotatory strengths are transformed into units of De and superimposed with Gaussian functions centred at the respective wavenumbers of the electronic transitions. An exponential half-width at 1/e peak height Ds = 0.4 eV was used for each gaussian curve (Stephens and Harada, 2009). Molecular structures were done with Molden software (Schaftenaar and Noordik, 2000).

In vitro anti-inflammatory assay. The *in vitro* anti-inflammatory assay is based on the ability of macrophages to generate a strong inflammatory response when stimulated with pro-inflammatory compounds. Mouse macrophages were stimulated by LPS from *E. coli* and exposed to the test material for 24 h. At the end of the incubation period, NO production was evaluated indirectly by measuring the accumulation of nitrite/nitrate, the stable end-products of NO oxidation, in the culture medium using a spectrophotometric method based on the Griess reaction. Immortalized mouse macrophages (RAW 264.7 cell line, Sigma-Aldrich), low passage number (<50) maintained in DMEM with stable L-glutamine supplemented with 10 % of inactivated calf serum, were seeded into 96-well tissue culture plates at the concentration of 1.10^5 cells/ml (200 µL/well) and incubated at 37 °C (5 % CO_2) for 24 h. At the end of the incubation period, the culture medium was decanted and replaced by 100 µL of medium containing the appropriate concentrations of the test material (8 different concentrations), and cells were incubated at 37 °C (5 % CO_2) for 1 h. At the end of the incubation period, pro-inflammatory LPS from *E. coli* was added to cell cultures (1 µg/mL). Then cells were incubated at 37 °C (5 % CO_2) for 24 h. Negative control DMSO, 1 % (*v/v*) and positive control dexamethasone were into each set of experiments, and results were obtained from triplicate in three independent experiments. NO release was measured in the culture supernatant by the Griess reaction. 50 µL of the supernatants were transferred into the wells of a 96-well tissue culture plate, and 50 µL of the Griess modified reagent (SIGMA) were added in each well. After a 15 min period at room temperature, the Optical Density (OD) of each well was read at 540 nm by a fluorescence-luminescence reader Infinite M200 Pro (TECAN). The results obtained for wells treated with the test material were compared to those of untreated control wells (DMSO) and converted to percentage values. In parallel to the assessment of NO release, cell viability was measured to validate the assay and to determine the selectivity index (SI) of the test material. The WST-1 vital dye reagent was used to measure cell mitochondrial respiration. For this purpose, the culture medium was decanted and 50 µL of WST-1 reagent (1/10 dilution) were added in each well. After a 30-min incubation period at 37 °C (5 % CO_2), the OD of each well was read at 450 nm by a fluorescence-luminescence reader Infinite M200 Pro (TECAN). The results obtained for wells treated with the test material were compared to those of untreated control wells (DMSO, 100 % viability) and converted to percentage values. The concentrations of the test material causing a 50 % release of cell viability (IC_{50}) and a 50 % of NO release (IC_{50} NO) were calculated using software Tablecurve Version 2.0. The anti-inflammatory ratio (selectivity index) corresponded to the ratio between the anti-inflammatory activity and the toxicity. It was expressed as follows: anti-inflammatory ratio = $IC_{50} \times 100/IC_{50}$ NO.

In vitro cytotoxic assay. HepG2 (human liver cancer) and HT29 (human colon and colorectal adenocarcinoma) cell lines were used to assess the toxicity of samples. In the performed assay, cytotoxicity was expressed as a concentration-dependent reduction of the uptake of the vital dye Neutral Red (NR) when measured 24 h after treatment. NR is a weak cationic dye that readily penetrates cell membranes by non-diffusion, accumulating intracellularly in lysosomes. Alterations of the cell surface of the sensitive lysosomal membrane lead to lysosomal fragility and other changes that gradually become irreversible. Such changes result in a decreased uptake and binding of NR in non-viable cells. HT29 (ATCC® HTB-38™) and HepG2 (ATCC® HTB-38™), low passage number (<50), were cultivated into DMEM (Dulbecco's Minimum Essential Medium, PAN BIOTECH. lot 1874561) supplemented with Penicillin 100 IU/mL and streptomycin 100 µg/mL (PAN BIOTECH, Lot 945514), and 10 % of inactivated calf serum (PAN BIOTECH, Lot P56314), pH 7.2, freshly prepared, stored no longer than 1 week. Cells were seeded into 96-well tissue culture plates (0.1 mL per well), at the concentration of 1.10^5 cells/mL, and incubated at 37 °C (5 % CO_2) until semi-confluent. The test material was diluted into sterile DMSO (stock solutions 0.1, 1 and 10 mg/mL) at final concentrations ranging from 0.1 to 250 µg/mL. The culture medium was decanted and replaced by 100 µL of fresh medium containing the various concentrations of the test material, then cells were incubated for 24 h at 37 °C (5 % CO_2). At the end of the incubation period, cells were placed into Neutral Red medium (50 µg/mL NR in complete medium) and incubated for 3 h at 37 °C, 5 % CO2. Then the medium was removed and cells were washed three times with 0.2 mL of HBSS to remove excessive dye. The Neutral Red medium was removed and the distaining solution (50 % ethanol, 1 % acetic acid,

49 % distilled water; 50 μL per well) was added into the wells. Then, the plates were shaken for 15–20 min at room temperature in the dark. AII the test samples and controls were run in triplicates in three independent experiments. The degree of membrane damage (*i.e.* the increase of released NR) was measured by a fluorescence-luminescence reader Infinite M200 Pro (TECAN). The Optical Density (OD) of each well was read at 540 nm. The results obtained for wells treated with the test material were compared to those of untreated control wells (HBSS, 100 % viability) and converted to percentage values. The concentrations of the test material causing a 50 % release of the preloaded NR (IC_{50}) as compared to the control culture were calculated using software Phototox Version 2.0. The mean OD value of blank wells (containing only NR desorbed solution) was subtracted from the mean OD value of three test/untreated wells.

Feature-Based Molecular Networking. The four crude extracts obtained from the red and the white phenotypes of *I. ammoxylum* (leaves and bark), as well as the 18 isolated compounds, were profiled by UHPLC-QqTOF-MS/MS in a mass range from *m/z* 50 to 1200, using positive (+) mode for the ESI source. The following parameters were used: end plate offset at 500 V; nebulizer gas pressure at 3.5 bar; dry gas flow at 12 L/min; drying temperature at 200 °C; acquisition rate at 4.0 Hz. The capillary voltage was set at 4500 V, with a fragmentation energy of 20–40 eV. The UHPLC conditions were as follows: sample concentrations: 5 mg/mL (crude extracts), 0.2 mg/mL (isolated compounds) in 100 % MeOH, injection volume: 2 μL, column temperature: 40 °C, elution gradient of H_2O–CH_3CN with 0.1 % HCO_2H (98:02 over 2 min, 98:02 to 0:100 over 12 min, 0:100 over 3 min) at a flow rate of 0.5 mL/min. Raw data obtained from the crude extracts analysis were converted into open format.mzXML using software Bruker Compass DataAnalysis Version 4.2 and processed using software Mzmine Version 2.53 (Olivon et al., 2017b; Pluskal et al., 2010; Smirnov et al., 2018). Then, a feature-based molecular network , combining data of the four crude extracts, was created on the GNPS platform (Wang et al., 2016) and is available following the link https://gnps.ucsd.edu/ProteoSAFe/status.jsp?task=1f11085b9ae740f2a45d5718024c7229. The Mzmine MS/MS data processing comprises.mzXML files import, MS peak detection, ADAP chromatogram builder, chromatogram deconvolution, isotopic peaks grouper, alignment, filtering, gap filling, fragment search, adduct search and spectra normalization. Setting parameters were as follows: positive ionization mode, centroid detection, MS1 peak detection limit: 1^E3, MS2 peak detection limit: 1^E2, *m/z* tolerance 10 ppm, peak/top edge ratio:2, peak duration range: 0.03–1 min, m/z range for MS2 pairing: 0.02 Da, RT range for MS2 pairing: 0.1 min, representative isotope: most intense, alignment weight for *m/z*: 75, weight for RT: 25, filtering RT tolerance: 0.1 min, filtering *m/z* tolerance: 0.001 *m/z*, adduct search $[M+Na]^+$, $[M + NH_4]^+$, spectra normalization type: average intensity. Processed files including a mgf and a csv file were uploaded to the GNPS platform. A metadata table was elaborated as a txt file and uploaded to the GNPS platform, in order to combine three different variables to the MN: phenotype (red/white), plant part (bark/leaves) and activity (selective/non-selective). A MN was then developed using the Advanced Analysis Tools – Feature Networking workflow (Nothias et al., 2020). Advanced Network Options parameters were as follows: Min pair cos: 0.7, minimum matched fragment ions: 6, network topK: 10, maximum connected component size: 100. The output was imported into Cytoscape Version 3.8.2, in order to visualize the network. Node annotations were performed manually for isolated compounds, and with GNPS spectral databases (score threshold: 0.7) and *In-Silico* MS/MS DataBase ISDB (score threshold: 0.2) (Allard et al., 2016).

Funding sources

This work was supported by European Regional Development Funds [GURDTI 2018-1828-0002370] (ERDF PHAR, EU-Région Réunion-French State national counterpart). Elise Gerometta was a recipient of a fellowship from the Région Réunion.

CRediT authorship contribution statement

Elise Gerometta: Writing – original draft, Methodology, Investigation, Formal analysis. **Elnur Garayev:** Writing – review & editing, Visualization, Validation, Methodology, Formal analysis. **Gaëtan Herbette:** Writing – review & editing, Visualization, Validation, Methodology, Formal analysis. **Arnaud Marvilliers:** Writing – review & editing, Methodology, Investigation, Formal analysis. **Carole Di Giorgio:** Writing – review & editing, Formal analysis. **Patricia Clerc:** Writing – review & editing, Formal analysis. **Michel Frederich:** Writing – review & editing, Visualization, Validation. **Béatrice Baghdikian:** Writing – review & editing, Visualization, Validation, Methodology. **Isabelle Grondin:** Writing – review & editing, Visualization, Validation, Supervision, Methodology, Conceptualization. **Anne Gauvin-Bialecki:** Writing – review & editing, Visualization, Validation, Supervision, Project administration, Methodology, Funding acquisition, Conceptualization.

Declaration of competing interest

The authors declare that they have no known competing financial interests or personal relationships that could have appeared to influence the work reported in this paper.

Data availability

NMR data are made freely available at https://doi.org/10.5281/zenodo.7092122. MS/MS data have been deposited on MassIVE (https://massive.ucsd.edu): MSV000089759.

Acknowledgements

Mr. H. Thomas (Parc National de La Réunion, La Plaine Des Palmistes 97431, La Réunion) is thanked for locating and identifying the investigated plant species and Mr. H. Hoarau (Conservatoire Botanique National Mascarin, Saint-Leu 97436, La Réunion) is thanked for the information about the red and white phenotypes. Dr. C. Simmler (IMBE), Dr. S. Greff (IMBE) and the Service of Chemical Ecology and Metabolomics (Aix-Marseille Université) are thanked for the acquisition of the LC/MSMS data. Dr. J-V. Naubron is thanked for the ECD experiments (Spectropole, Aix-Marseille Université).

Appendix A. Supplementary data

Supplementary data to this article can be found online at https://doi.org/10.1016/j.phytochem.2024.114005.

References

Allard, P.-M., Péresse, T., Bisson, J., Gindro, K., Marcourt, L., Pham, V.C., Roussi, F., Litaudon, M., Wolfender, J.-L., 2016. Integration of molecular networking and *in-silico* MS/MS fragmentation for natural products dereplication. Anal. Chem. 88, 3317–3323. https://doi.org/10.1021/acs.analchem.5b04804.

Almabruk, K.H., Chang, J.H., Mahmud, T., 2016. Total synthesis of (±)-Isoperbergins and correction of the chemical structure of perbergin. J. Nat. Prod. 79, 2391–2396. https://doi.org/10.1021/acs.jnatprod.6b00621.

Batterham, T.J., Highet, R.J., 1963. Nuclear magnetic resonance spectra of flavonoids. Aust. J. Chem. 17, 428–439.

Becke, A.D., 1993. Density-functional thermochemistry. III. The role of exact exchange. J. Chem. Phys. 98, 5648–5652. https://doi.org/10.1063/1.464913.

Belofsky, G., Carreno, R., Lewis, K., Ball, A., Casadei, G., Tegos, G.P., 2006. Metabolites of the “smoke tree”, *Dalea spinosa* , potentiate antibiotic activity against multidrug-resistant *Staphylococcus aureus*. J. Nat. Prod. 69, 261–264. https://doi.org/10.1021/np058057s.

Bojase, G., Wanjala, C.C.W., Majinda, R.R.T., 2001. Two new isoflavanoids from Bolusanthus speciosus. Bull. Chem. Soc. Ethiop. 15, 131–136.

Campos, J.K.L., Araújo, T.F. da S., Brito, T.G. da S., Silva, A.P.S. da, Cunha, R.X. da, Martins, M.B., Silva, N.H., da, Santos, B.S., dos, Silva, C.A., da, Lima, V.L. de M., 2018. *Indigofera suffruticosa* mill. (Anil): plant profile, phytochemistry, and pharmacology review. Advances in Pharmacological Sciences 2018. https://doi.org/10.1155/2018/8168526, 1–6.

Cheeseman, J.R., Trucks, G.W., Keith, T.A., Frisch, M.J., 1996. A comparison of models for calculating nuclear magnetic resonance shielding tensors. J. Chem. Phys. 104, 5497–5509. https://doi.org/10.1063/1.471789.

Cho, I.-A., You, S.-J., Kang, K.-R., Kim, S.-G., Oh, J.-S., You, J.-S., Lee, G.-J., Seo, Y.-S., Kim, D.K., Kim, C.S., Lee, S.-Y., Kim, J.-S., 2017. Biochanin-A induces apoptosis and suppresses migration in FaDu human pharynx squamous carcinoma cells. Oncol. Rep. 38, 2985–2992. https://doi.org/10.3892/or.2017.5953.

de Almeida, J.G.L., Silveira, E.R., Pessoa, O.D.L., 2008. NMR spectral assignments of a new [C-O-C] isoflavone dimer from *Andira surinamensis*. Magn. Reson. Chem. 46, 103–106. https://doi.org/10.1002/mrc.2138.

Ding, H.-Y., Chiang, C.-M., Tzeng, W.-M., Chang, T.-S., 2015. Identification of 3′-hydroxygenistein as a potent melanogenesis inhibitor from biotransformation of genistein by recombinant Pichia pastoris. Process Biochem. 50, 1614–1617. https://doi.org/10.1016/j.procbio.2015.06.007.

Dorla, E., Grondin, I., Hue, T., Clerc, P., Dumas, S., Gauvin-Bialecki, A., Laurent, P., 2019. Traditional uses, antimicrobial and acaricidal activities of 20 plants selected among Reunion Island's flora. South Afr. J. Bot. 122, 447–456. https://doi.org/10.1016/j.sajb.2018.04.014.

Elmi, A., Spina, R., Abdoul-Latif, F., Yagi, S., Fontanay, S., Risler, A., Duval, R.E., Laurain-Mattar, D., 2018. Rapid screening for bioactive natural compounds in Indigofera caerulea Rox fruits. Ind. Crop. Prod. 125, 123–130. https://doi.org/10.1016/j.indcrop.2018.08.089.

Felix, F.B., Vago, J.P., Fernandes, D. de O., Martins, D.G., Moreira, I.Z., Gonçalves, W.A., Costa, W.C., Araújo, J.M.D., Queiroz-Junior, C.M., Campolina-Silva, G.H., Soriani, F. M., Sousa, L.P., Grespan, R., Teixeira, M.M., Pinho, V., 2021. Biochanin A regulates key steps of inflammation resolution in a model of antigen-induced arthritis via GPR30/PKA-dependent mechanism. Front. Pharmacol. 12, 662308 https://doi.org/10.3389/fphar.2021.662308.

Fontaine, C., Lavergne, C., 2007. Indigofera ammoxylum (DC.) Polhill - Plan directeur de conservation : outils d'aide à la conservation des espèces végétales menacées d'extinction. Conservatoire Botanique National de Mascarin, Saint-Leu.

Frisch, M.J., Trucks, G.W., Schlegel, H.B., Scuseria, G.E., Robb, M.A., Cheeseman, J.R., Scalmani, G., Barone, V., Mennucci, B., Petersson, G.A., Nakatsuji, H., 2013. Gaussian 09, Revision D.01. Gaussian Inc.

Gerometta, E., Grondin, I., Smadja, J., Frederich, M., Gauvin-Bialecki, A., 2020. A review of traditional uses, phytochemistry and pharmacology of the genus Indigofera. J. Ethnopharmacol. 253, 112608 https://doi.org/10.1016/j.jep.2020.112608.

Herath, H.M.T.B., Dassanayake, R.S., Priyadarshani, A.M.A., De Silva, S., Wannigama, G. P., Jamie, J., 1998. Isoflavonoids and a pterocarpan from Gliricidia sepium. Phytochemistry 47, 117–119. https://doi.org/10.1016/S0031-9422(97)00517-7.

Ingham, J.L., Dewick, P.M., 1979. A new isoflavan phytoalexin from leaflets of Lotus hispidus. Phytochemistry 18, 1711–1714. https://doi.org/10.1016/0031-9422(79)80190-9.

Jurd, L., Manners, G.D., 1977. Isoflavene, isoflavan, and flavonoid constituents of gliricidia sepium. J. Agric. Food Chem. 25, 723–726. https://doi.org/10.1021/jf60212a034.

Küpeli, E., Tatli, I.I., Akdemir, Z.S., Yesilada, E., 2007. Estimation of antinociceptive and anti-inflammatory activity on Geranium pratense subsp. finitimum and its phenolic compounds. J. Ethnopharmacol. 114, 234–240. https://doi.org/10.1016/j.jep.2007.08.005.

Ledoux, A., Cao, M., Jansen, O., Mamede, L., Campos, P.-E., Payet, B., Clerc, P., Grondin, I., Girard-Valenciennes, E., Hermann, T., Litaudon, M., Vanderheydt, C., Delang, L., Neyts, J., Leyssen, P., Frédérich, M., Smadja, J., 2018. Antiplasmodial, anti-chikungunya virus and antioxidant activities of 64 endemic plants from the Mascarene Islands. Int. J. Antimicrob. Agents 52, 622–628. https://doi.org/10.1016/j.ijantimicag.2018.07.017.

Li, W., Liu, F., Zhang, P., 2008. Synthesis of isoflavones via base catalysed condensation reaction of deoxybenzoin. J. Chem. Res. 2008, 683–685. https://doi.org/10.3184/030823408X382135.

Liu, L.-F., Li, W.-H., Li, M.-Y., Wu, X.-Z., Yang, F., Xu, J.-N., Yuan, C.-S., 2020. Chemical constituents from common vetch (*Vicia sativa* L.) and their antioxidant and cytotoxic activities. Nat. Prod. Res. 34, 3205–3211. https://doi.org/10.1080/14786419.2018.1560282.

Luiz-Ferreira, A., Cola, M., Barbastefano, V., de-Faria, F., Almeida, A., Farias-Silva, E., Calvo, T., Hiruma-Lima, C., Vilegas, W., Souza-Brito, A., 2012. Healing, antioxidant and cytoprotective properties of Indigofera truxillensis in different models of gastric ulcer in rats. Indian J. Manag. Sci. 13, 14973–14991. https://doi.org/10.3390/ijms131114973.

Nothias, L.F., Petras, D., Schmid, R., Dührkop, K., Rainer, J., Sarvepalli, A., Protsyuk, I., Ernst, M., Tsugawa, H., Fleischauer, M., Aicheler, F., Aksenov, A., Alka, O., Allard, P.-M., Barsch, A., Cachet, X., Caraballo, M., Da Silva, R.R., Dang, T., Garg, N., Gauglitz, J.M., Gurevich, A., Isaac, G., Jarmusch, A.K., Kameník, Z., Kang, K.B., Kessler, N., Koester, I., Korf, A., Gouellec, A.L., Ludwig, M., Christian, M.H., McCall, L.-I., McSayles, J., Meyer, S.W., Mohimani, H., Morsy, M., Moyne, O., Neumann, S., Neuweger, H., Nguyen, N.H., Nothias-Esposito, M., Paolini, J., Phelan, V.V., Pluskal, T., Quinn, R.A., Rogers, S., Shrestha, B., Tripathi, A., van der Hooft, J.J.J., Vargas, F., Weldon, K.C., Witting, M., Yang, H., Zhang, Z., Zubeil, F., Kohlbacher, O., Böcker, S., Alexandrov, T., Bandeira, N., Wang, M., Dorrestein, P.C., 2020. Feature-based molecular networking in the GNPS analysis environment. Nat. Methods 17, 905–908. https://doi.org/10.1038/s41592-020-0933-6.

Olivon, F., Allard, P.-M., Koval, A., Righi, D., Genta-Jouve, G., Neyts, J., Apel, C., Pannecouque, C., Nothias, L.-F., Cachet, X., Marcourt, L., Roussi, F., Katanaev, V.L., Touboul, D., Wolfender, J.-L., Litaudon, M., 2017a. Bioactive natural products prioritization using massive multi-informational molecular networks. ACS Chem. Biol. 12, 2644–2651. https://doi.org/10.1021/acschembio.7b00413.

Olivon, F., Grelier, G., Roussi, F., Litaudon, M., Touboul, D., 2017b. MZmine 2 data-preprocessing to enhance molecular networking reliability. Anal. Chem. 89, 7836–7840. https://doi.org/10.1021/acs.analchem.7b01563.

Pluskal, T., Castillo, S., Villar-Briones, A., Orešič, M., 2010. MZmine 2: modular framework for processing, visualizing, and analyzing mass spectrometry-based molecular profile data. BMC Bioinf. 11, 395. https://doi.org/10.1186/1471-2105-11-395.

Rahman, T.U., Uddin, G., Nisa, R.U., Ludwig, R., Liaqat, W., Mahmood, T., Mohammad, G., Choudhary, M.I., Ayub, K., 2015. Spectroscopic and density functional theory studies of 7-hydroxy-3′-methoxyisoflavone: a new isoflavone from the seeds of Indigofera heterantha (Wall). Spectrochim. Acta Mol. Biomol. Spectrosc. 148, 375–381. https://doi.org/10.1016/j.saa.2015.04.018.

Schaftenaar, G., Noordik, J.H., 2000. Molden: a pre- and post-processing program for molecular and electronic structures. J. Comput. Aided Mol. Des. 14, 123–134.

Shawl, A.S., Vishwapaul, Zaman, A., Kalla, A.K., 1984. Isoflavones of Iris spuria. Phytochemistry 23, 2405–2406. https://doi.org/10.1016/S0031-9422(00)80573-7.

Shen, T., Xie, C.-F., Wang, X.-N., Lou, H.-X., 2013. Stilbenoids. In: Ramawat, K.G., Mérillon, J.-M. (Eds.), Natural Products. Springer Berlin Heidelberg, Berlin, Heidelberg, pp. 1901–1949. https://doi.org/10.1007/978-3-642-22144-6_63.

Smirnov, A., Jia, W., Walker, D.I., Jones, D.P., Du, X., 2018. ADAP-GC 3.2: graphical software tool for efficient spectral deconvolution of gas chromatography–high-resolution mass spectrometry Metabolomics data. J. Proteome Res. 17, 470–478. https://doi.org/10.1021/acs.jproteome.7b00633.

Stephens, P.J., Devlin, F.J., Chabalowski, C.F., Frisch, M.J., 1994. Ab initio calculation of vibrational absorption and circular dichroism spectra using density functional force fields. J. Phys. Chem. 98, 11623–11627. https://doi.org/10.1021/j100096a001.

Stephens, P.J., Harada, N., 2009. ECD cotton effect approximated by the Gaussian curve and other methods. Chirality NA-NA. https://doi.org/10.1002/chir.20733.

Su, X., Huang, Q., Chen, J., Wang, M., Pan, H., Wang, R., Zhou, H., Zhou, Z., Liu, J., Yang, F., Li, T., Liu, L., 2016. Calycosin suppresses expression of pro-inflammatory cytokines via the activation of p62/Nrf2-linked heme oxygenase 1 in rheumatoid arthritis synovial fibroblasts. Pharmacol. Res. 113, 695–704. https://doi.org/10.1016/j.phrs.2016.09.031.

Su, Z., Wang, P., Yuan, W., Grant, G., Li, S., 2017. Phenolics from the fruits of *Maclura pomifera*. Nat. Prod. Commun. 12, 1934578X1701201 https://doi.org/10.1177/1934578X1701201122.

Su, Z., Wang, P., Yuan, W., Li, S., 2013. Flavonoids and 3-arylcoumarin from pterocarpus soyauxii. Planta Med. 79, 487–491. https://doi.org/10.1055/s-0032-1328297.

Sundarrajan, S., Arumugam, M., 2017. A systems pharmacology perspective to decipher the mechanism of action of Parangichakkai chooranam , a Siddha formulation for the treatment of psoriasis. Biomed. Pharmacother. 88, 74–86. https://doi.org/10.1016/j.biopha.2016.12.135.

Tanaka, T., Ohyama, M., Iinuma, M., Shirataki, Y., Komatsu, M., Charles, L.B., 1998. Isoflavonoids from Sophora secundiflora, S. arizonica and S. gypsophila. Phytochemistry 48, 1187–1193. https://doi.org/10.1016/S0031-9422(97)00802-9.

Técher, S., 2013. Criblage d'activités biologiques de plantes endémiques ou indigènes de La Réunion - Recherche de molécules antivirales ciblant le virus du chikungunya. Université de La Réunion.

Umehara, K., Nemoto, K., Kimijima, K., Matsushita, A., Terada, E., Monthakantirat, O., De-Eknamkul, W., Miyase, T., Warashina, T., Degawa, M., Noguchi, H., 2008. Estrogenic constituents of the heartwood of Dalbergia parviflora. Phytochemistry 69, 546–552. https://doi.org/10.1016/j.phytochem.2007.07.011.

Umehara, K., Nemoto, K., Matsushita, A., Terada, E., Monthakantirat, O., De-Eknamkul, W., Miyase, T., Warashina, T., Degawa, M., Noguchi, H., 2009. Flavonoids from the heartwood of the Thai medicinal plant *Dalbergia parviflora* and their effects on estrogenic-responsive human breast cancer cells. J. Nat. Prod. 72, 2163–2168. https://doi.org/10.1021/np900676y.

Wang, M., Carver, J.J., Phelan, V.V., Sanchez, L.M., Garg, N., Peng, Y., Nguyen, D.D., Watrous, J., Kapono, C.A., Luzzatto-Knaan, T., Porto, C., Bouslimani, A., Melnik, A. V., Meehan, M.J., Liu, W.-T., Crüsemann, M., Boudreau, P.D., Esquenazi, E., Sandoval-Calderón, M., Kersten, R.D., Pace, L.A., Quinn, R.A., Duncan, K.R., Hsu, C.-C., Floros, D.J., Gavilan, R.G., Kleigrewe, K., Northen, T., Dutton, R.J., Parrot, D., Carlson, E.E., Aigle, B., Michelsen, C.F., Jelsbak, L., Sohlenkamp, C., Pevzner, P., Edlund, A., McLean, J., Piel, J., Murphy, B.T., Gerwick, L., Liaw, C.-C., Yang, Y.-L., Humpf, H.-U., Maansson, M., Keyzers, R.A., Sims, A.C., Johnson, A.R., Sidebottom, A.M., Sedio, B.E., Klitgaard, A., Larson, C.B., Boya P, C.A., Torres-Mendoza, D., Gonzalez, D.J., Silva, D.B., Marques, L.M., Demarque, D.P., Pociute, E., O'Neill, E.C., Briand, E., Helfrich, E.J.N., Granatosky, E.A., Glukhov, E., Ryffel, F., Houson, H., Mohimani, H., Kharbush, J.J., Zeng, Y., Vorholt, J.A., Kurita, K.L., Charusanti, P., McPhail, K.L., Nielsen, K.F., Vuong, L., Elfeki, M., Traxler, M.F., Engene, N., Koyama, N., Vining, O.B., Baric, R., Silva, R.R., Mascuch, S.J., Tomasi, S., Jenkins, S., Macherla, V., Hoffman, T., Agarwal, V., Williams, P.G., Dai, J., Neupane, R., Gurr, J., Rodríguez, A.M.C., Lamsa, A., Zhang, C., Dorrestein, K., Duggan, B.M., Almaliti, J., Allard, P.-M., Phapale, P., Nothias, L.-F., Alexandrov, T., Litaudon, M., Wolfender, J.-L., Kyle, J.E., Metz, T.O., Peryea, T., Nguyen, D.-T., VanLeer, D., Shinn, P., Jadhav, A., Müller, R., Waters, K.M., Shi, W., Liu, X., Zhang, L., Knight, R., Jensen, P.R., Palsson, B.Ø., Pogliano, K., Linington, R. G., Gutiérrez, M., Lopes, N.P., Gerwick, W.H., Moore, B.S., Dorrestein, P.C., Bandeira, N., 2016. Sharing and community curation of mass spectrometry data with global natural products social molecular networking. Nat. Biotechnol. 34, 828–837. https://doi.org/10.1038/nbt.3597.

Zhang, X.-X., Zhang, Z.-X., Chen, L., Su, Y.-F., 2006. New aliphatic nitro-compounds from Indigofera carlesii. Fitoterapia 77, 15–18. https://doi.org/10.1016/j.fitote.2005.06.015.